Study on Thermal and Mechanical Properties of 2D Silicon Carbide using Molecular Dynamics Simulation

By

Abu Syed Md. Jannatul Islam

A thesis submitted in partial fulfillment of the requirements for the degree of Master of Science in Engineering in the Department of Electrical and Electronic Engineering

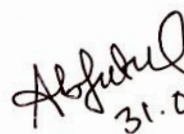Khulna University of Engineering & Technology
Khulna 920300, Bangladesh

January 2019

Declaration

This is to certify that the thesis work entitled *"Study on Thermal and Mechanical Properties of 2D Silicon Carbide using Molecular Dynamics Simulation"* has been carried out by *Abu Syed Md. Jannatul Islam* in the Department of *Electrical and Electronic Engineering*, Khulna University of Engineering & Technology, Khulna, Bangladesh. The above thesis work or any part of this work has not been submitted anywhere for the award of any degree or diploma.

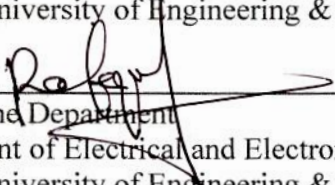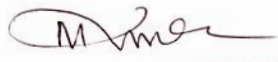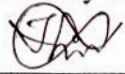31.01.19

Signature of Supervisor

31.01.19

Signature of Candidate

Approval

This is to certify that the thesis work submitted by *Abu Syed Md. Jannatul Islam* entitled "*Study on Thermal and Mechanical Properties of 2D Silicon Carbide using Molecular Dynamics Simulation*" has been approved by the board of examiners for the partial fulfillment of the requirements for the degree of *Master of Science in Electrical & Electronic Engineering* in the Department of *Electrical and Electronic Engineering*, Khulna University of Engineering & Technology, Khulna-9203, Bangladesh in January 2019.

BOARD OF EXAMINERS

1. _____ 31-01-19
Dr. Md. Sherajul Islam
Professor
Department of Electrical and Electronic Engineering
Khulna University of Engineering & Technology

Chairman
(Supervisor)

2. _____
Head of the Department
Department of Electrical and Electronic Engineering
Khulna University of Engineering & Technology

Member

3. _____
Dr. Md. Rafiqul Islam (1)
Professor
Department of Electrical and Electronic Engineering
Khulna University of Engineering & Technology

Member

4. _____
Dr. Md. Jahirul Islam
Assistant Professor
Department of Electrical and Electronic Engineering
Khulna University of Engineering & Technology

Member

5. _____
Dr. Anisul Haque
Professor
Department of Electrical and Electronic Engineering
East West University

Member
(External)

Acknowledgement

All approvals belong to the Almighty **ALLAH**, the most kind hearted and bounteous to all **HIS** creatures and their actions. I humbly praise and grateful to **HIM, WHO** permits me to live and accomplish tasks including the research work being presented in this thesis.

I would like to thank my thesis supervisor, **Dr. Md. Sherajul Islam**, Professor, Department of Electrical and Electronic Engineering (EEE), Khulna University of Engineering & Technology (KUET), Bangladesh, for his continuous supervision, encouragements, precious guidance, advices and helps, constructive criticisms and keen interests throughout the progress of the work. It is hard to imagine how I would move from knowing nothing to the thermal and mechanical properties of 2D-SiC materials without his guidance and patience. I believe that work with him is a grand opportunity and would be a never-ending memory.

I would also like to thank Prof. Dr. Asharaful Ghani Bhuiyan and Prof. Dr. Md. Rafiqul Islam (2) for their motivational instructions in different perspective of my thesis work and for other things to fulfill the requirements of good research.

I want to thank all my respected teachers and many of my friends outside my research field, for who I would not list the names but who have painted wonderful colors to the sky of my research life.

Last but not the least, I would like to thank my beloved parents and brothers for their continuous encouragement during the hard times of my thesis work and for supporting me in every step of my educational life to build up my career in the field of EEE.

Abstract

Recently, two dimensional silicon carbide (2D-SiC) is expected to be a promising semiconductor for nanoelectronics and nanoelectromechanical systems (NEMS) due its exceptional electronic, thermal and mechanical properties. Although numerous studies have been performed on the characterization of structural and electronic properties of 2D-SiC, the thermal and mechanical behaviors have not been well studied. In this dissertation, non-equilibrium molecular dynamics simulation has been performed to explore the thermal properties of 2D-SiC. Moreover, the mechanical behaviors of 2D-SiC are quantified using the virial stress based molecular dynamics simulation.

This dissertation provides many new important findings based on these simulations such as a slowly decreasing trend of thermal conductivity in the high temperature region, deviating the $\sim 1/T$ law due to the influence of high frequency phonons and Umklapp limited phonon scattering. The simulated thermal conductivity of 2D-SiC using optimized tersoff potential is found as ~ 271.03 W/mK at a length of 600 nm which is one order higher than silicene of the same length. However, due to the lower acoustic group velocities, lower Debye temperature, and additional phonon scattering effect of the binary SiC system, the reported thermal conductivity is much lower than graphene. The phonon density of states (PDOS) shows a strengthening behavior of the low frequency acoustic peaks with the increase of sheet length, quantifies the increasing trend of thermal conductivity with length at room temperature. Above room temperature a shrinking trend of acoustic phonon peaks is noticed, conveys the causes of decreasing trend of thermal conductivity with temperature. However, due to the consideration of ground state phonon modes in specific heat capacity, the quantum corrected thermal conductivity shows an increasing trend up to Debye limit. In addition, it is found that the optimized tersoff potential provides a better estimation of the thermal conductivity than the original tersoff potential due to proper parameterization of the SiC system with analytical model.

Further, the mechanical behaviors of pristine and defected 2D-SiC have been studied. The effect of point, bi, and mixed vacancy defects on the tensile strength and elastic modulus have been determined. The estimated tensile strength and elastic modulus of pristine 2D-SiC show a linear reduction trend with temperature due to the strong thermal variation effect. For pristine 2D-SiC, a tensile strength of 53.625 ± 7 GPa with a failure strain of 0.153 is found at room temperature. However, with the introduction of vacancy defects, the tensile strength and

elastic modulus of 2D-SiC reduces significantly due to the symmetry breakdown and the bond breaking effect. Among the three types of vacancy, the point vacancy shows the most treacherous effect on the tensile strength and elastic modulus due its greater bond breaking effect. It is found that for 1%-point vacancy, the tensile strength is reduced about 66.35% from that of pristine case. Therefore, these findings are very much important to understand new phonon transport physics and potentially lead to not only in nanoelectronics and nanoelectromechanical systems, but also in novel applications of 2D-SiC in various emerging fields.

Dedicated To

My Beloved Parents & Respected Teachers

Contents

LIST OF FIGURES

LIST OF TABLES

LIST OF ILLUSTRATIONS

eV	Electron-volt
SiC	Silicon Carbide
1D	One dimensional
2D	Two dimensional
MD	Molecular Dynamics
EMD	Equilibrium Molecular Dynamics
NEMD	Non-equilibrium Molecular Dynamics
NEMS	Nanoelectromechanical system
PBC	Periodic Boundary Condition
h-BN	Hexagonal Boron Nitrite
CNT	Carbon nanotube
PDOS	Phonon Density of State
LO	Longitudinal Optic mode phonon
TO	Transverse Optic mode phonon
ZO	Cross-plane or Flexural Optic mode phonon
LA	Longitudinal Acoustic mode phonon
TA	Transverse Acoustic mode phonon
ZA	Cross-plane or Flexural Acoustic mode phonon
LD	Lattice Dynamics
AGF	Atomistic Green Function
BTE	Boltzmann Transport Equation
ps	picoseconds
fs	femtoseconds
PBC	Periodic Boundary Conditions
LAMMPS	Large-scale Atomic/Molecular Massively Parallel Simulator
OVITO	Open Visualization Tool
HCACF	Heat Current Autocorrelation Function

NOMENCLATURE

v	Velocity
T	Temperature
N	No. of atoms
E_{total}	Total Energy
U_{total}	Total Potential Energy
r_{ij}	Distance between particles i and j
$\phi(r_{ij})$	Potential energy between particles i and j
ρ_i	Local electron density
$V^R(r_{ij})$	Pair-wise repulsion force
$V^A(r_{ij})$	Pair-wise attraction force
bij	Bond order between atom i and j
N_f	Total translational degrees of freedom of the system
v_i^{α}	Velocity of atom α in i direction
K	Thermal conductivity
K_B	Boltzmann constant
Δt	MD simulation time step
ΔQ	Small amount of heat
M	Heat energy exchange frequency
A	Cross-sectional area
h	Sheet thickness
T_D	Debye temperature

CHAPTER I

Introduction and Research Objectives

1.1 Introduction

Heat elimination is a major problem in nanoelectronic devices. Due to the increased number of transistor integration in per unit area, there occurs significant heat generation in the devices, which creates localized hot spots and high temperature gradients [1, 2], and both of which reduces the reliability and scale down trend of transistors. Therefore, to maintain the miniaturization trend of logic circuits and transistors [3], and satisfying Moore's Law in the upcoming future it is important to explore new nanomaterials [4] or new device architectures to solve the thermal management problem efficiently. Along with thermal management problem the mechanical stability issue is an another important concern in present day nanoelectromechanical systems (NEMS) [5]. Different environmental conditions as well as the unavoidable defect formation during fabrication processes greatly affect the mechanical performances of the nanoscale devices and systems. Therefore, a novel nanomaterial with unique electronic, thermal, and mechanical properties is an urgent need for the realization of next generation nanoelectronics.

Over the last two decades, an extensive research attention has been paid to synthesize novel nanostructures based on two dimensional (2D) materials. Among the hundreds of 2D materials that have been successfully synthesized e.g. graphene, silicene, h-BN, SiC, GaN, ZnO, Phosphorene, TMDs [6-13] etc., graphene [14] the first 2D nanosheet of carbon atoms shows extraordinary thermal, mechanical, and electronic properties [15]. Moreover, silicene [16], the silicon equivalent of carbon atoms, has recently become a new popular 2D material due to its Dirac electronic dispersion at the Fermi level [10] and superior compatibility with the existing Si-based electronics. However, both the graphene and silicene demonstrates zero bandgap, which make them unaffordable for the electronic device applications. Though the other 2D nanomaterials show considerable electronic bandgap, it is desirable to appreciate for such type of 2D nanomaterials, which have strong in-plane covalent bonds to resist large mechanical deformation as well as very high thermal conductivity to transport the phonon particles smoothly at different environmental conditions.

In this admiration, 2D silicon carbide (SiC) –a binary compound of silicon and carbon atoms– has gained extensive research attention recently due to its device applicable bandgap of ~2.53 eV [17], and inherent robust structure like graphene and silicene [18]. 2D-SiC is also expected to show other novel physical properties such as high excitonic binding energy of ~2.0 eV [17, 19], Bose-Einstein effect [20], carrier doped spin adjusting [21], and bandgap tuning through strain engineering [22], for instance. These exceptional properties make 2D-SiC a favorable candidate for nanoelectronics, solar cells, LEDs, spintronics, nano-sensors, and nano-composites applications. [17, 19, 23] Furthermore, due to the large mechanical strength, high thermal conductivity, high chemical stability, high stiffness, high melting temperature, and other valuable properties of bulk counterparts [24], the novel 2D-SiC is predicted to be used in harsh environment, oxidized and corrosive atmosphere [24] to create nanoelectromechanical systems (NEMS). On the basis of these unusual features, Glenn Research Centre at National Aeronautics and Space Administration agency (NASA), USA is raising exertions to develop silicon carbide (SiC) as the next generation nanomaterial for advanced semiconductor device applications. They have informed that SiC based devices have constantly revealed suitable operation at temperatures as high as 923 K which is in contrast to conventional silicon based equipments which can only work up to 623 K [25]. To think about the applicability, recently, T. Susi et al. [26] reported the experimental synthesis of 2D-SiC using atomic resolution scanning electron microscopy. Moreover, *ab-initio* calculations [17, 27, 28] further support the dynamic and thermal stability of the monolayer SiC structure. Therefore, 2D-SiC is expected to be a promising semiconductor nanomaterial for both fundamental research and wide range of applications in nanoelectronic and optoelectronic devices in near future. Some of the proposed applications of SiC in different devices and systems are shown in Fig. 1.1.

Although 2D-SiC is predicted to have the potentials for a wide range of applications due its superior properties, the studies on the 2D-SiC are just limited to several structural and electronic properties [26, 28, 29] only. For the realization of nanoscale systems with improved performance compared to conventional silicon-based electronics, an in-depth investigation of thermal properties of 2D-SiC is very much essential. Moreover, to apply the 2D-SiC into NEMS, nano-composites, electronic/optical interconnects, and in microelectromechanical components [30], the mechanical behavior characterization is also indispensable. Therefore, a detailed

understanding of thermal and mechanical properties is urgently needed for the practical applications of 2D-SiC.
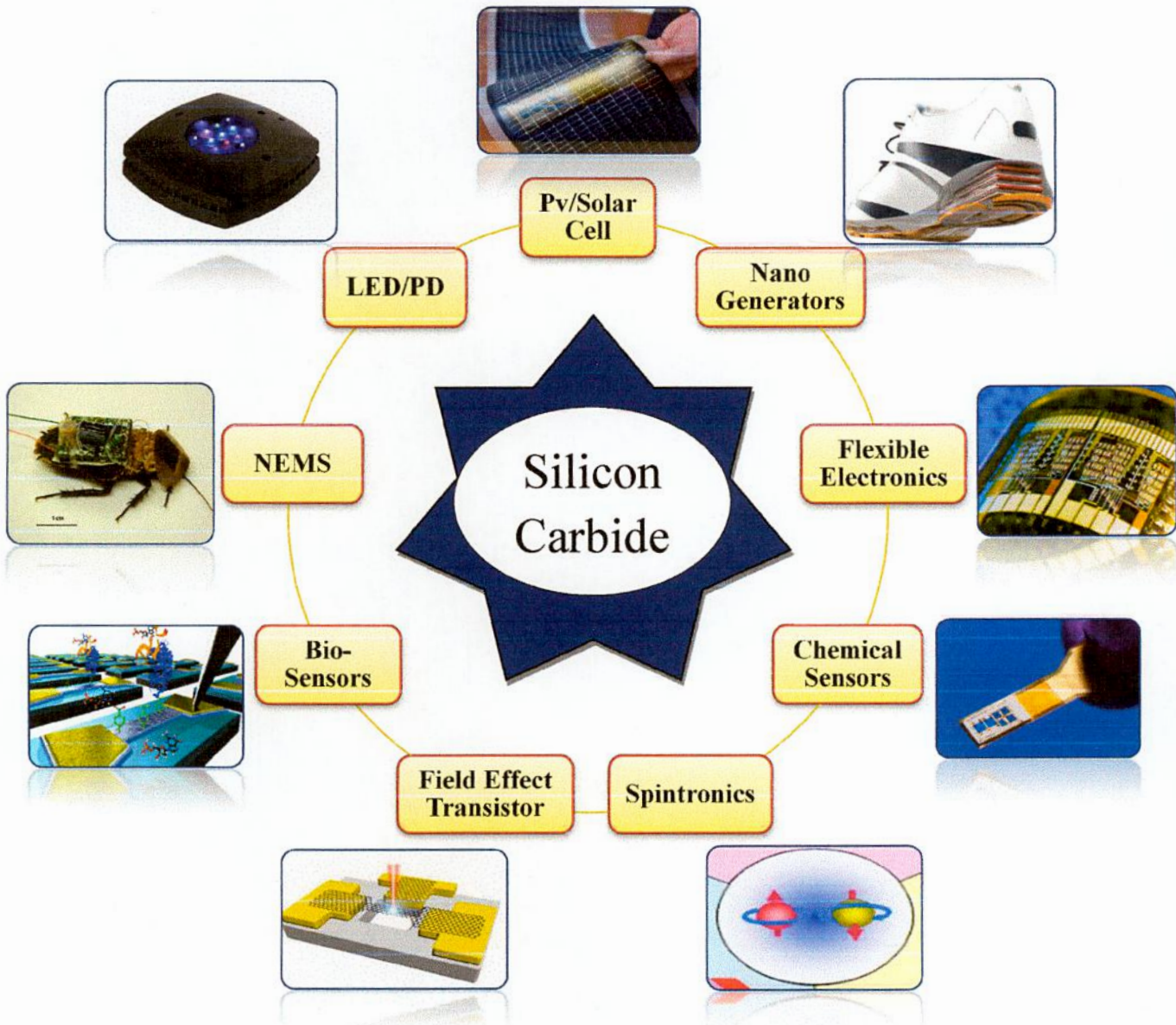
Figure 1.1: Some expected applications of 2D-SiC in different devices and systems.

1.2 Motivation

In recent years, the rapid growth of 2D nanomaterials initiates a great revolution in the semiconductor industry to ensure the miniaturization trend [32] of nanoelectronics. However, when devices or systems are turned into nanoscale range [33, 34], heat management as well as structural stability is a great issue that hampers the successful operation of nanoscale devices and systems [4, 36]. Therefore, for the development of next generation field-effect transistors [36], interconnects [37], and composite substrates [38], the proper characterization of thermal conductivity and mechanical strength of nanomaterials with different geometry and environmental conditions is a fundamental apprehension in present day nanoresearch.

Of late, 2D–SiC is predicted to be a novel nanomaterial with intriguing electronic, thermal and mechanical properties that can be used to solve the heat dissipation as well as the mechanical stability problem of nanoscale systems. However, when materials are moved from bulk to low dimensional systems such as 2D or 1D (nanorings or nanotubes) systems, their electronic, thermal and mechanical properties change significantly and it is very much important to characterize these properties with reliable techniques. In recent years, thermal properties of different 2D materials such as graphene [31, 39], boron nitride [40], and molybdenum disulfide [41], have been intensively studied. From these studies, it has been found that phonons- the quanta of lattice vibration, in quasi one-dimensional systems (1D) such as carbon nanotube and boron nitride nanotube, and 2D systems such as graphene and boron nitride, behave otherwise and can conduct heat more efficiently than their bulk counterparts [41]. It is also found that the material's ability to transport heat is solely depends on their constituent atoms, geometrical shapes and environmental conditions [35, 42]. Therefore, nanowires do not conduct heat as well as bulk crystals owing to the greater phonon-boundary scattering [43] or changes in the phonon dispersion [44] characteristics. On the other hand, theoretical studies of heat conduction in two-dimensional (2D) and one-dimensional (1D) crystals has revealed unusual behavior that leads to infinitely large intrinsic thermal conductivity [45] and divergence nature due to the dissimilar behavior of phonons from their bulk equivalents. Besides, in 2D systems the phonon anharmonicity alone is not sufficient for restoring thermal equilibrium, and one needs to either limit the system size or introduce disorder to have the physically meaningful finite value of thermal conductivity [46]. Therefore, as nanostructures can show very different properties when

compared with their bulk colleagues, it is crucial to investigate the phonons behavior and thermal properties of this newly synthesized 2D-SiC sheet under different circumstances.

Moreover, in nano-composites, and NEMS related applications, structural stability is a great issue [5, 47]. It is reported that, with the increase of temperature the mechanical strength of many 2D materials [5, 47] is reduced significantly. Therefore, to implement this novel 2D-SiC into nano-sensors, nano-composites and nanomechanical systems, it is important to study its mechanical performances in different temperature conditions. Furthermore, from a realistic point of view, when materials are fabricated from their bulk structure or synthesized experimentally, there occurs different types of defects like a point vacancy defect, bi-vacancy defect, stone-wales defect, ad-atoms defect, isotope defect etc. [48-50]. These defects can significantly change the structural strength of the nanomaterials [51-53]. Accordingly, when the 2D-SiC is synthesized, it is also despoiled with different types of vacancy defects. These vacancy defects like point vacancy, bi-vacancy and mixed vacancy can reduce the tensile strength, elastic modulus and other mechanical properties of the 2D-SiC monolayer. Therefore, it is also important to explore the effects of different vacancy defects on the mechanical properties of 2D-SiC sheet.

However, compared to the structural and electronic properties of 2D-SiC [26, 28, 29], very little is known about its thermal and mechanical properties. Recently, Guo *et al.* [54] has calculated the strain dependent thermal conductivity of the monolayer SiC sheet at room temperature condition using the first principles calculations. This study explores that the thermal conductivity of 2D-SiC is two orders of magnitude lower than that of graphene [55] due to its small group velocity and short phonon lifetimes. An anomalous tempestuous behavior in the thermal conductivity with the increase of strain is also observed from this report. However, to deal with the heat management at different temperature circumstances, temperature dependent thermal conductivity calculation of 2D-SiC is a great concern in nanoelectronics. Nevertheless, to the best of our knowledge, there is no study on the temperature dependence of thermal properties of 2D-SiC. In 2D nanostructures such as graphene, stanene, black phosphorene, silicene etc. [56, 58], the thermal conductivity usually follows the *1/T* law with temperature. Moreover, for the newly synthesized 2D GaN and ZnO sheets [59-61], an unusual slowly decreasing trend of thermal conductivity with temperature is observed due to the dominant contribution of optical phonons in thermal transport. Therefore, an intriguing thermal behavior

with wide temperature ranges is also expected as well from this Si and C based binary compound. Besides, in low dimensional systems the thermal transport behavior is largely dependent on the system length [62, 63]. For example, the thermal conductivity in carbon nanotube (CNT) exposes power law behavior while for monolayer graphene the thermal conductivity shows logarithmic nature [31, 64, 65] with system length. The investigation of length dependent thermal transportation is thus of great significance for fundamental research and technological applications. However, at room temperature to a higher temperature, how the phonons play a role to conduct heat and how their density of states varies with length are unknown. Therefore, an in-depth understanding of heat transport phenomenon of 2D-SiC at different length and temperature conditions is an important task to solve the challenges of nanoscale systems.

On the other hand, a large number of studies have been performed to explore the mechanical behaviors of SiC systems at different temperature and defect conditions. However, these works are limited to SiC nanowires, nanorods, nanotubes and for cubic crystal systems [66-68] only. Recently, quasi-2D, 2D-SiC and SiC_2 systems [29, 69, 70] have been synthesized and the mechanical behavior of Si_mC_n sheet for Stone-Wales defect and for different concentration of Si atom are explored using the Molecular Dynamic Finite Element Method (MDFEM) [71-73]. From these studies, it is found that the mechanical properties of the SiC sheets are relatively high when the silicon concentration is low or silicon atoms are well dispersed and reduction in fracture properties depends on the tensile direction as well as the orientation of Stone-Wales defects. However, to the best of our knowledge, there is no study on the mechanical properties of 2D-SiC considering distinct as well as the combined effects of randomly distributed vacancy defects with different temperature conditions. Furthermore, there is no study on varying concentrations of randomly distributed point vacancy, bi-vacancy and mixed vacancy defects. Therefore, an in-depth understanding of the mechanical behaviors of vacancy defected 2D-SiC sheet at different temperature with varying concentration of vacancy is an urgent need for the realization of next generation nanoelectromechanical systems.

To investigate the underlying physical mechanism of heat transport and mechanical strength in low-dimensional materials, many atomistic simulation techniques have been developed in the last decade. Due to the simple crystal structure of 2D materials and increased

computational efficiency, molecular dynamics (MD) simulations [76], non-equilibrium Green's function (NEGF) [78], Boltzmann transport equation (BTE) [79], First Principles calculations [59], and continuum mechanics models [83] takes great position in the characterization of various physical properties of the nanomaterials. On the other hand, experimental studies on low dimensional materials, especially 2D materials, are relatively rare, due to the challenges in suspending nanomaterials suitable for thermal measurements and in measuring the temperature distribution in nano/micro scale. Moreover, in experimental techniques, measurement of mechanical behaviors with different types of realistic defects is also very challenging. Hence, numerical approach with greater reliability as well as accuracy and large scale simulation is the most appreciable to explore the physical properties of the nanoscale systems.

1.3 Objectives

To fulfill the requirements of nanoelectronics and nanoelectromechanical systems, the newly synthesized 2D-SiC is predicted to open a new era due to its unique electronic, thermal, and mechanical properties. The thermal properties of any nanomaterials are significantly influenced by the size and temperature. The mechanical behavior of nanosheet is also modified due to the temperature and vacancy defects. Therefore, to quantify the thermal transport phenomena and mechanical properties of the novel 2D-SiC, the main objectives of this dissertation have been spun in the following headings:

I   To quantify the thermal conductivity of the 2D-SiC sheet at different length and temperature conditions using non-equilibrium molecular dynamics simulation.

II To probe the phonon modes for quantitive explanation of the thermal conductivity at different length and temperature conditions using velocity auto-correlation of atoms.

III To explore the thermal conductivity behavior of 2D-SiC below and above the Debye temperature limit using quantum correction.

IV To investigate the effect of parameterization on the thermal conductivity of the 2D-SiC sheet at different length and temperature conditions using original and optimized tersoff potential.

V   To discover the mechanical behavior such as tensile strength and elastic modulus of the pristine 2D-SiC sheet at different temperature conditions.

VI	To study the impact of randomly distributed point vacancy, bi-vacancy and mixed vacancy defects on the mechanical properties of 2D-SiC sheet at different temperature.
VII	To determine the tensile strength and elastic modulus of 2D-SiC sheet for randomly distributed vacancy defect concentration at room temperature.

1.4 Synopsis of Dissertation

Chapter 2 gives an overview of the basic concepts of 2D-SiC and summarizes the simulation fundamentals for the thermal and mechanical property evaluation of nanomaterials. It also gives a description about the classical molecular dynamics simulation (MD) approach, the LAMMPS software for MD simulation and OVITO software for MD visualization.

Chapter 3 focuses on the computational methods, specially Reverse Non-equilibrium Molecular Dynamics Simulation (RNEMD) to explore the thermal conductivity; Fourier transformation of the velocity auto-correlation of atoms to calculate the phonon density of states; Virial stress theorem to calculate the mechanical properties of 2D-SiC.

Chapter 4 shows the results- the thermal, mechanical and phonon properties of 2D-SiC. The impact of temperature, length and interatomic potential on the thermal conductivity is given here. Furthermore, the effect of point vacancy, bi-vacancy, mixed vacancy and temperature on the mechanical behaviors of 2D-SiC are also presented here.

Finally, **Chapter 5** provides a summary of the most relevant results, combined with an outlook on possible future research directions.

CHAPTER II

Material and Simulation Fundamentals

2.1 Introduction

This chapter is intended to provide an overview and introduction about the fundamental perceptions of the newly synthesized two dimensional silicon carbide material. Moreover, a detailed description about the essentials of the novel molecular dynamics (MD) simulation technique which is used in this dissertation to explore the physical properties such as thermal conductivity and mechanical behaviors of the 2D-SiC is described here in details. Finally, the procedures of implementation of this MD simulation using the open source (large atomic molecular massively parallel simulator) LAMMPS and (open visualization tool) OVITO packages are shown with proper explanation.

2.2 Fundamentals of Silicon Carbide

2.2.1 Bulk Silicon Carbide

Bulk silicon carbide (SiC) –a binary compound of silicon and carbon atoms– is a promising semiconductor material, convenient for high temperature and high power device applications due to its extraordinary thermal, mechanical, chemical, and wide band gap properties [74]. Therefore, synthesize of the low dimensional SiC and its characterization in different aspects has become a hot topics in nanotechnology to achieve benefits from it. Unlike the polymorphs of carbon, SiC is a polar material. Irrespective of the fact that, although both the constituents of SiC are group IV elements, charges in SiC system are moved from Si to C atoms due to the higher electronegativity of the C atom. Furthermore, in bulk SiC there are six stacking arrangements indicated as 3C zincblende, 2H wurtzite, 4H-SiC, 6H-SiC, 15R-SiC, and 21R-SiC. Before going to 2D –SiC, some basic things such as crystal structure, electronic dispersion and phonon dispersion curves of the zincblende and wurzite SiC crystals are shown in Fig. 2.1. From the figures, it has been found that the bulk SiC is an indirect bandgap semiconductor and it has six phonon branches such as LA, TA, ZA, LO, TO, and ZO modes.

Bulk SiC

SiC 3D Zincblende

$E_C = 12.939$ eV; $E_G = 1.41$ eV
$E_G(+GW_0) = 2.40$ eV

SiC 3D Wurtzite

$E_C = 12.933$ eV; $E_G = 2.36$
$E_G(+GW_0) = 3.32$ eV

Energy Bands

Phonon Modes
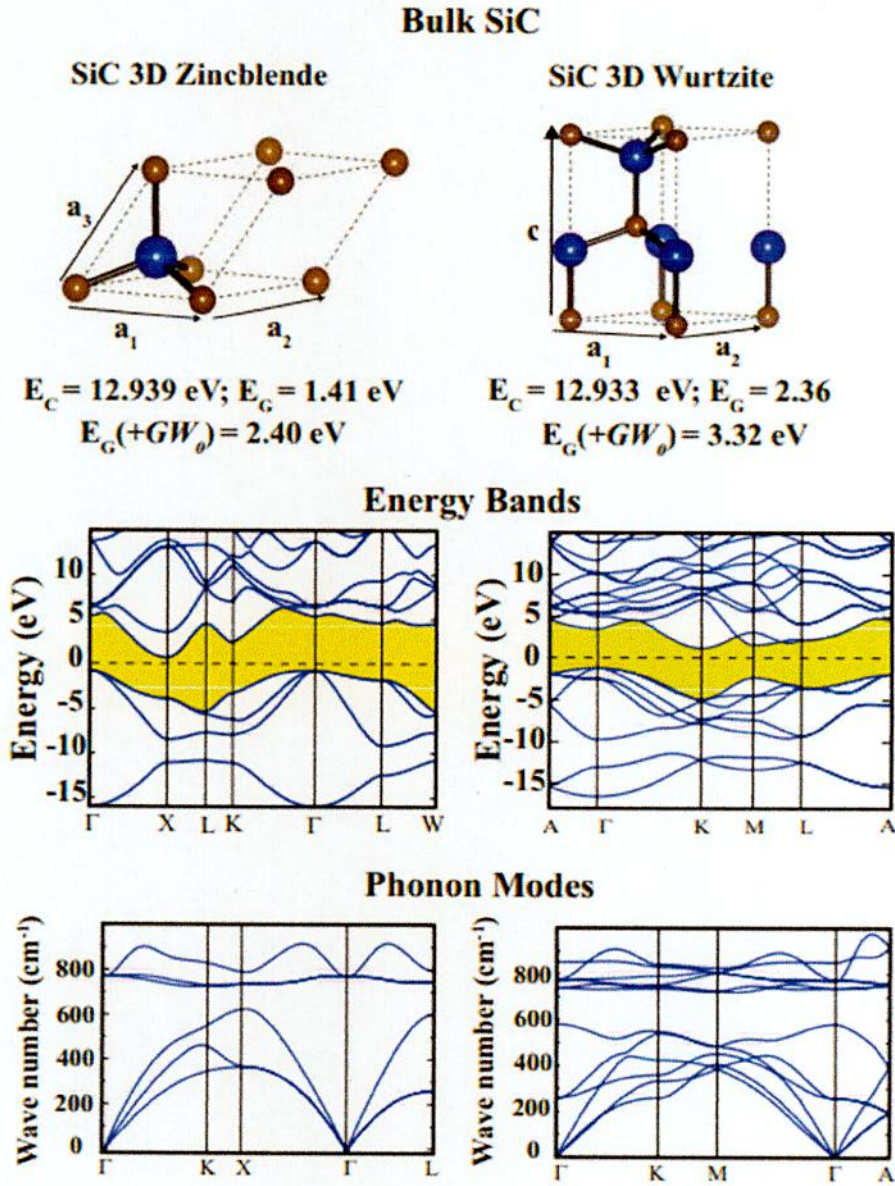
Figure 2.1: Crystal Structure of 3D Zincblende and Wurzite SiC with their electronic as well as phonon dispersion behavior [77].

2.2.2 2D Silicon Carbide

Although graphene the 2D form of graphite shows a stable planar crystal structure, the 2D planar form of Si system is unstable. It is reported that, it can be stabilized through puckering technique [10]. Therefore, the honeycomb arrangement is same to both Si and C atoms and one can assume

for the stable 2D structure of the SiC system. Of late, it has been reported that there occurs a lot of theoretical [27, 75, 76] studies to explore the energy landscape of 2D Si_xC_y $(x,y \in N)$ sheets. Moreover, some groups performed experimental works [26, 29] to synthesize the nano-sized SiC materials. These theoretical as well as experimental investigations informed that, 2D-SiC can be really possible to synthesize and it is a stable structure with sp^2 hybridized planar crystal. In Fig. 2.3 the electronic band structure of 2D-SiC is presented along with that of silicene and graphene. From the figure, it is found that 2D-SiC is a binary compound and it shows a direct K point bandgap of ~2.52 eV due to its iconicity [23]. Again the bond length of Si to C atoms has an impact on the bandgap properties. As seen from Fig. 2.4, monolayer SiC would transit from direct into indirect bandgap semiconductor (namely $\Delta_{KK} > \Delta_{KM}$) when bond length is less than 1.74 Å. From Fig. 2.4b it is seen that, when the bond length varies within the range of 1.74 to 2.0 Å, the monolayer SiC shows a direct bandgap ($\Delta_{KK} < \Delta_{KM}$).

The honeycomb 2D-SiC unit cell can be thought of a graphene like unit cell with one carbon atom replaced by a silicon atom which is shown in Fig. 2.2. The dynamically favorable buckling free planar structure can be found when Si-C bond length is in between 1.74 Å to 2.0 Å, larger than the equivalent C–C bonds in graphene (1.42 A°). The Si–C–Si and C–Si–C bond angles are 120°. The 2D-SiC is produced by the sp^2 orbital hybridization combining σ-bonds and π-bonds.

Top View   **Side View**
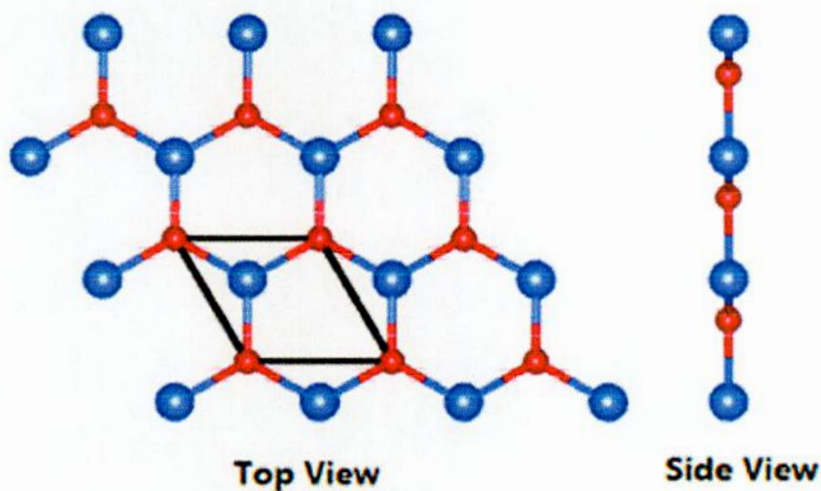
Figure 2.2: Monolayer 2D-SiC sheet.
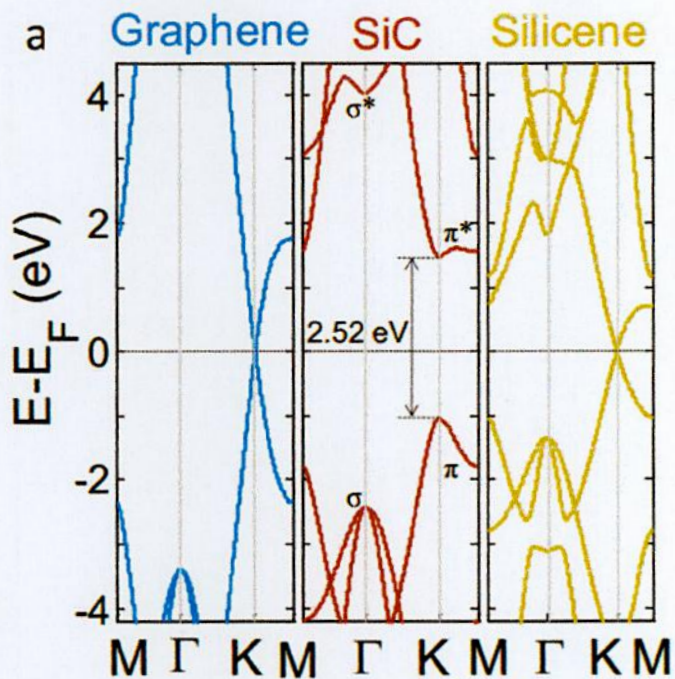
Figure 2.3: Electronic dispersion curves for 2D Graphene, SiC, and Silicene [79].
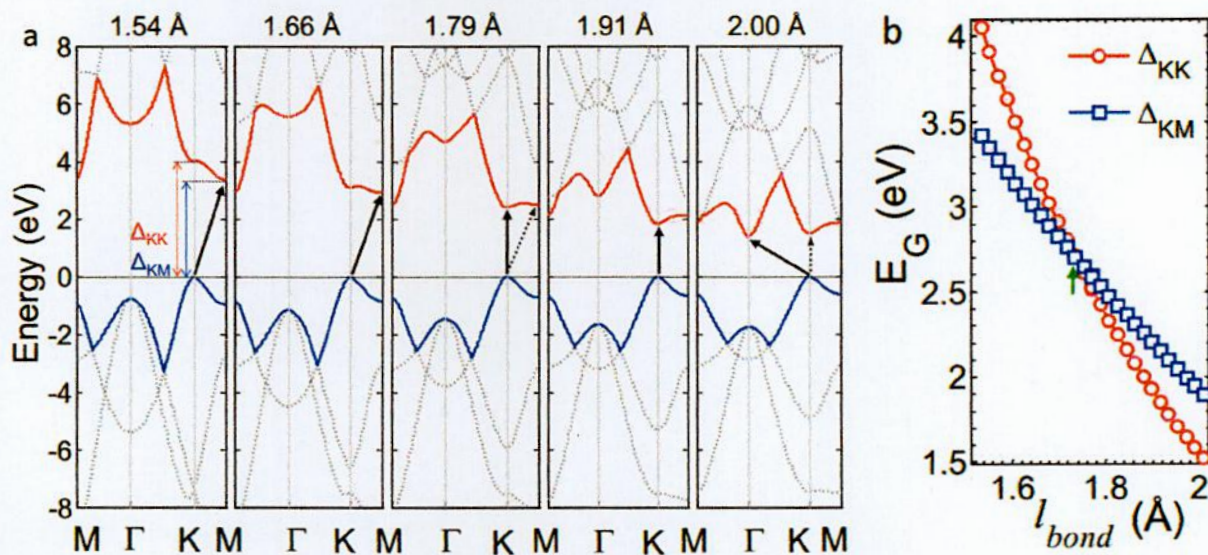
Figure 2.4: Effect of bond length (l_{bond}) variation on the Electronic dispersion curve of 2D-SiC [79].

The phonon dispersion relation and phonon density of states of 2D-SiC are shown in Fig. 2.5 (a) and (b), respectively. As the 2D-SiC contains two types of atoms (Si and C), there produces six phonon branches such as three acoustic (LA, TA, ZA) phonons and three optical (LO, TO, ZO) phonons in the phonon-dispersion curve. Among these phonon branches, the ZO and LO modes are the high frequency phonons which have a negligible impact on the heat transport of 2D-SiC reported by SD Guo et al. [54] Thus, for 2D-SiC the main heat carriers are LA, TA, ZA and ZO mode phonons. The phonon-dispersion provides no imaginary frequencies, which specifies that the 2D-SiC is thermodynamically stable. From the results, it is noticeably understood that there occurs a phonon band gap of 249.17 cm^{-1}, splitting the TO and LO branches from the ZO, LA, TA and ZA branches. This type of phonon band gap may be produced due to the variation of the atomic masses of Si and C atoms. Moreover, near the K point the LA and TA branches are linear, while ZA branch deviates from the linearity. In 2D-SiC, thus the phonon modes such as LA and TA attained a higher group velocity than the ZA mode phonons due to the linear dispersion behavior at low frequency region.
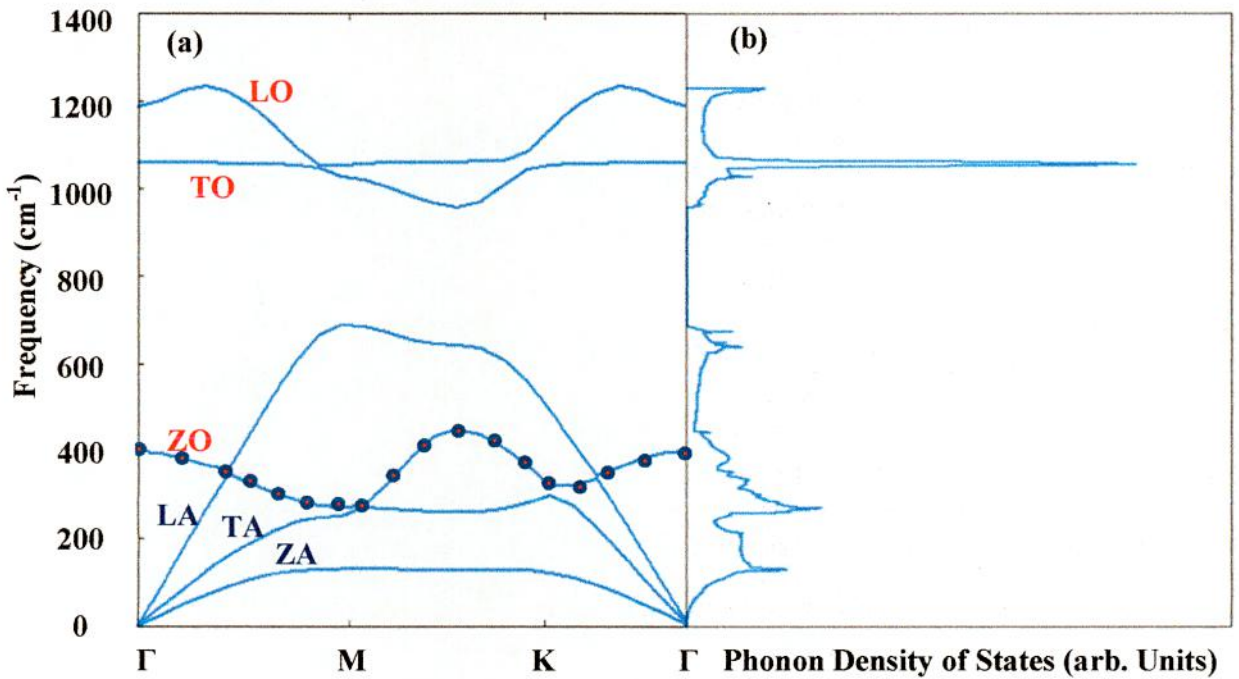
Figure 2.5: (a) Phonon dispersion relationship with Ultra-soft pseudo-potential using first principle density function theory, and (b) Corresponding Phonon Density of State of 2D-SiC.

As a result, the LA and TA mode phonons contribute a large in the heat transport than the ZA modes phonon which can be easily noticed from the quadratic dispersion behavior of Fig. 2.5. These fundamental things (structural and electronic properties) are really very much important as these things conveys the information which will be required when the thermal and mechanical properties of the 2D-SiC system is calculated.

2.3 Classical Molecular Dynamics Simulation

Classical Molecular Dynamics (MD) simulation (First reported by Alder + Wainwright in 1957) is a technique [80] used to simulate the motion of atoms, molecules, clusters, and even macroscopic systems such as gases, liquids and solids under predefined conditions. Therefore, it can be used to study the dynamical processes at the nanoscale range to calculate a broad range of properties, e.g. phase diagrams, diffusion coefficients, or various response functions, as well as static quantities such as radial distribution functions, coordination numbers, elastic moduli etc.

MD simulation, essentially employs the numerical solution of Newton's equations of motion for a set of atoms from a specified initial arrangement. The new positions and velocities of the atoms are acquired using a numerical integration technique such as velocity-verlet method [81]. This is commonly achieved via numerical integration by discretizing time into small intervals called the time step. The interactions between the atoms, i.e. the interatomic forces can be calculated based on various methods, ranging from density functional theory (DFT) to classical potentials. These forces control the spurt of the atoms and allow propagating the positions and velocities towards the next time step. Repeating this procedure many times yields a series of snapshots, describing the trajectory of the system in phase space, which can be analyzed to extract the desired properties.

2.3.1 Mathematical Explanation of MD Simulation

Newton's equation of motion is known as

$$F_i = m_i a_i \tag{2.1}$$

where, F_i denotes the applied force on particle i, m_i represents the mass of particle i and a_i is the acceleration of particle i. The force can also be stated as the gradient of the potential energy,
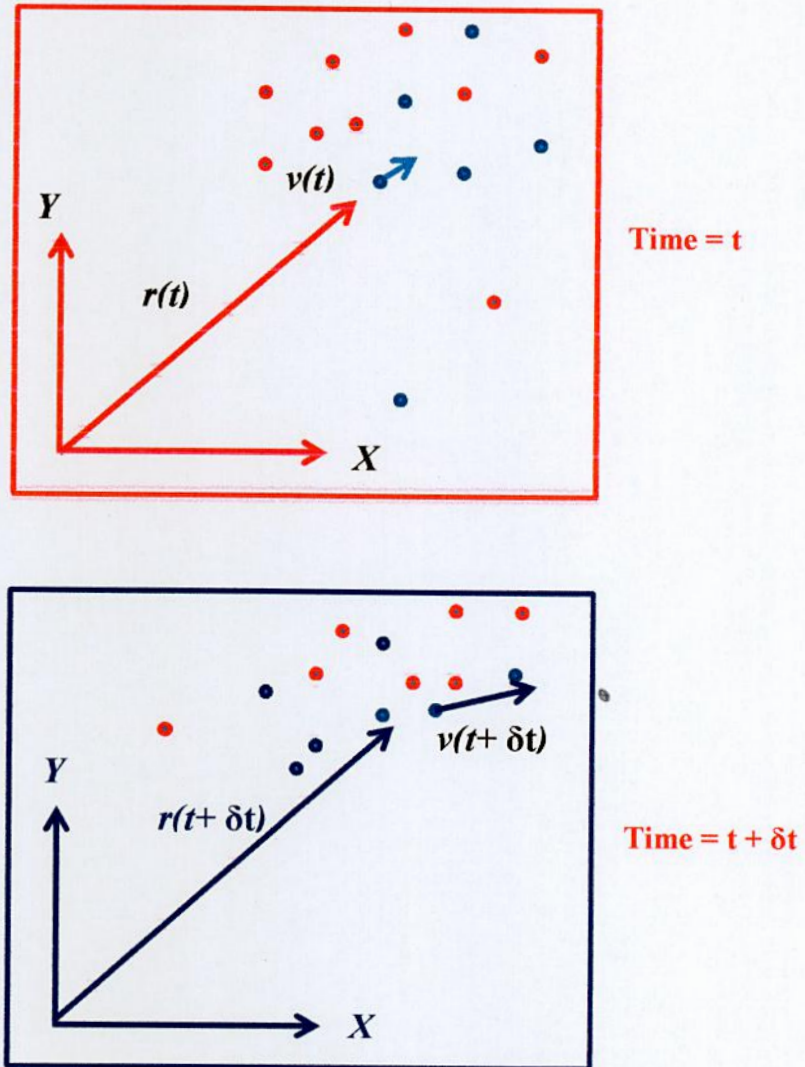
Figure 2.6: Variation of positions and velocities of an atom with time.

$$F_i = -\nabla_i V \qquad (2.2)$$

Combining these two equations yields

$$\frac{dV}{dr_i} = -m_i \frac{d^2 r_i}{dt^2} \qquad (2.3)$$

where, V represents the potential energy of the system.

Furthermore, the Newton's Second Law of motion can be expressed as follows

$$F = m \cdot a = m \cdot \frac{dV}{dt} = m \cdot \frac{d^2x}{dt^2} \qquad (2.4)$$

Taking the simple case where the acceleration is constant,

$$a = \frac{dV}{dt} \qquad (2.5)$$

An expression for the velocity after integration can be obtained as

$$v = at + v_0 \qquad (2.6)$$

and since

$$v = \frac{dx}{dt} \qquad (2.7)$$

Once again integration can be performed to obtain,

$$x = vt + x_0 \qquad (2.8)$$

Combining the output of Eqn. 2.8 with the expression for the velocity, it is possible to attain the resulting relation which provides the value of x at time t as a function of the acceleration, a, the initial position, x_0, and the initial velocity, v_0...

$$x = \frac{1}{2} * a * t^2 + v_0 * t + x_0 \qquad (2.9)$$

Using derivation of the potential energy in regard to the position, r, the acceleration can be described as

$$a = -\frac{1}{m}\frac{dE}{dr} \qquad (2.10)$$
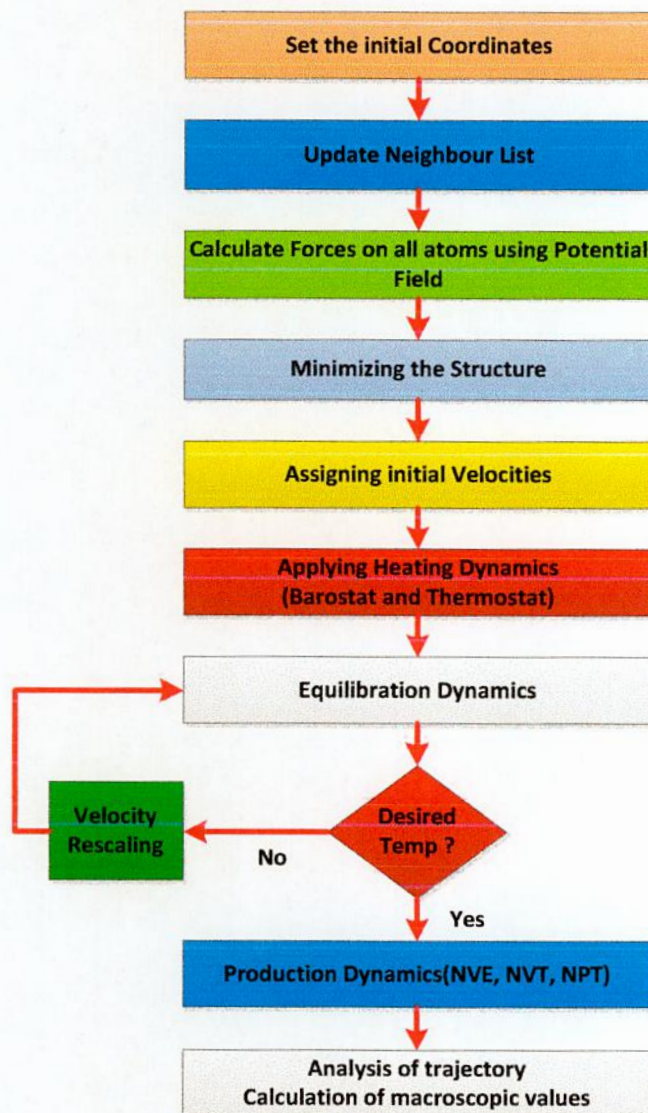
Figure 2.7: Flowchart of Molecular Dynamics Simulation

2.3.2 Classical Potentials in MD Simulation

Classical potential is considered as the heart in the MD simulation. It is used to describe the interaction among particles of a system. In chemistry and biology this is usually referred as Force-field and in material physics, it is Interatomic/ Empirical/ Analytical potentials. The objective of interatomic potentials or force fields is to give mathematical or analytical expressions that guess the energy scene of a large atomic system. The total potential energy can be expressed as:

$$E_{tot} = E_{covalent} + E_{non-covalent} \tag{2.11}$$

Where, E_{tot}, $E_{covalent}$, and $E_{non-covalent}$ are the total energy, covalent energy, and non-covalent energy, respectively. The components of covalent and non-covalent energies can be further broken down as,

$$E_{covalent} = E_{bond} + E_{angle} + E_{dihedral} + E_{out-of-plane} \tag{2.12}$$

$$E_{non-covalent} = E_{electrostatic} + E_{Vander\,Waals} \tag{2.13}$$

The many body analytical bond-order potentials used here for atomic scale simulation is proposed by Albe *et al.* [92]. The basic formulas that are used to calculate these potentials are discussed here. The cohesive energy can be expressed as:

$$E = \sum_{i>j} f_C \big[(r_{ij}) - \overline{b_{ij}} V_A(r_{ij}) \big] \tag{2.14}$$

and the attractive and repulsive contributions are

$$V_R(r) = (D_0/(S-1)) exp \big[-\beta\sqrt{2S}(r-r_0) \big] \tag{2.15}$$

$$V_A(r) = (SD_0/(S-1)) exp \big[-\beta\sqrt{2S}(r-r_0) \big] \tag{2.16}$$

where D_0 and r_0 are the dimer energy and bond length. β can be determined from the ground-state vibrational frequency of the dimer and S is adjusted to the slope of the Pauling plot.

The cutoff function

$$f_C(r) = \begin{cases} 1 & r < R-D \\ 1/2 - 1/2 \sin\left(\pi/2\frac{r-R}{D}\right) & |R-r| \le D \\ 0 & R+D < r \end{cases} \tag{2.17}$$

R and D specify the position and the width of the cutoff region. The bond-order is specified by

$$b_{ij} = (1+\chi_{ij})^{-1/2} \tag{2.18}$$

$$\chi_{ij} = \sum_{k(\neq i,j)} f_C(r_{ik}) exp\big[2\mu(r_{ij}-r_{ik})\big]g(\theta_{ijk}) \tag{2.19}$$

$$g(\theta) = \gamma\left(1 + \frac{c^2}{d^2} - \frac{c^2}{d^2+[h+cos\theta]^2}\right) \tag{2.20}$$

The three-body interactions are determined by the parameters 2μ, γ, c, d, and h, which leads in total to up to nine adjustable parameters, all of them depending on the type of atoms i and j.

Optimized	C	C	C	2	0.15	4.18426232	2019.8449
Original	Si	Si	Si	2.85	0.15	2.4799	1830.8
Optimized	Si	Si	Si	2.82	0.14	2.83318929	2145.7128
Original	C	Si	Si	2.35726	0.1527	2.9839	1597.311
Optimized	C	Si	Si	2.4	0.2	3.26563307	1779.36144
Original	C	Si	C	1.95	0.15	0	0
Optimized	C	Si	C	2	0.15	0	0
Original	C	C	Si	2.35726	0.15271	0	0
Optimized	C	C	Si	2.4	0.2	0	0
Original	Si	C	C	2.35726	0.1527	2.9839	1597.31114
Optimized	Si	C	C	2.4	0.2	3.26563307	1779.36144
Original	Si	Si	C	2.35726	0.15271	0	0
Optimized	Si	Si	C	2.4	0.2	0	0
Original	Si	C	Si	2.85	0.15	0	0
Optimized	Si	C	Si	2.82	0.14	0	0

2.3.3 Ensembles of MD Simulation

An ensemble is a collection of all possible systems which have different microscopic states, but have an identical macroscopic or thermodynamic state. Although integrating Newton's equations of motion allows exploring the constant-energy surface of a system, it is a general issue to keep the temperature and pressure of the system constant during the molecular simulation, to mimic experimental conditions. Therefore, MD simulation provides several methods for controlling the temperature and pressure. Depending on the parameters such as N (no. of atoms), V (Volume of the system), T (Temperature of the system), E (Energy of the system), and P (Pressure of the system), MD simulation may acquire NVE, NVT, and NPT ensembles.
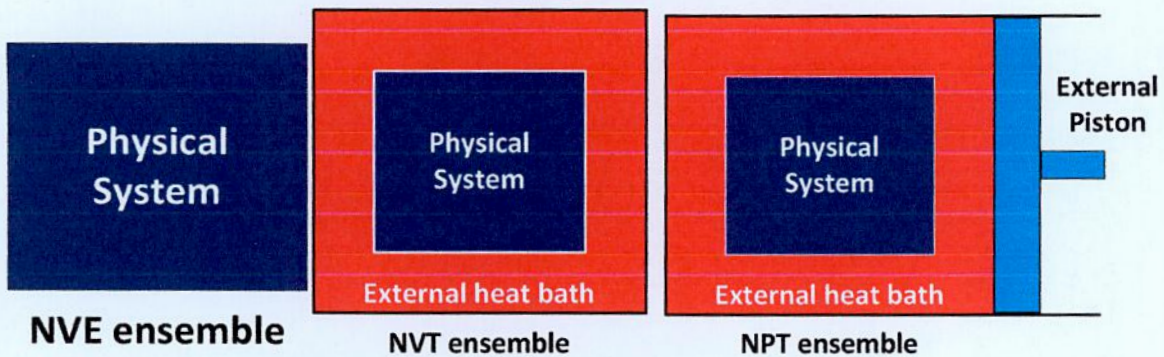
Figure 2.8: Block diagram of NVE, NVT and NPT ensembles.

2.3.4 Numerical Algorithms for Integration

Numerous numerical algorithms have been developed for integrating the equations of motion. Some of them are given here.

- Verlet algorithm
- Leap-frog algorithm
- Velocity Verlet algorithm
- Beeman's algorithm

2.3.4.1 The Velocity-verlet Algorithm

The new positions and velocities of the atoms are obtained using a numerical integration method such as Velocity-verlet method. According to the Velocity-verlet method,

$$r(t + \delta t) = r(t) + v(t)\delta t + \frac{1}{2}a(t)\delta t^2 \tag{2.21}$$

$$v(t + \delta t) = v(t) + \frac{1}{2}[a(t) + a(t + \delta t)]\delta t \tag{2.22}$$

Where r, v, and a are the position, velocity, and acceleration of an atom, respectively; t is the initial time; Δt is the time step. This algorithm yields positions, velocities and accelerations at time t. There is no compromise on precision.

2.3.5 Time Step

In MD simulation, the smallest period of time between two consecutive iterations is defined as time step. To get higher computational efficiency, larger time step must be needed while for increased accuracy of the simulation, a smaller time step is suggested. A time step should be less than 10% of the vibration period of an atom and, time step of 0.5 *fs* to 0.8 *fs* provides good results in 1D or 2D materials simulation. However, researchers have used time steps from 0.1 *fs* to 1 *fs* to simulate uniaxial tensile tests of 2D materials.

2.3.6 Strain Rate

In MD simulation, uniaxial or biaxial tensile tests are achieved by applying strain to the nanostructure at a constant strain rate. Researchers have found that the failure point of 2D materials depends on the strain rate [5]. At lower strain rates, the system has more time to relax

and reach an equilibrium state, and hence the results would be more accurate. Practical strain rates, used in experiments, such as $10^2 s^{-1}$ is not possible to simulate in MD simulations due to high computational time. Therefore, in order to become computationally viable, strain rate of the order of 10^9 is generally used in MD simulations. Researchers have used various strain rates ranging from 0.0005 ps^{-1} to 0.01 ps^{-1}.

2.3.7 Periodic Boundary Conditions

The most efficient way to simulate an infinitely large system is the use of periodic boundary conditions (PBC). In PBC, the cubical simulation box is replicated throughout space to form an infinite lattice as shown for a 2-D case in Fig. 2.9. During the simulation, when a molecule moves in the central box, its periodic images in every other box also move in exactly the same way. Thus, as a molecule leaves the central box, one of its images will enter through the opposite face. Therefore, the system has no edges.
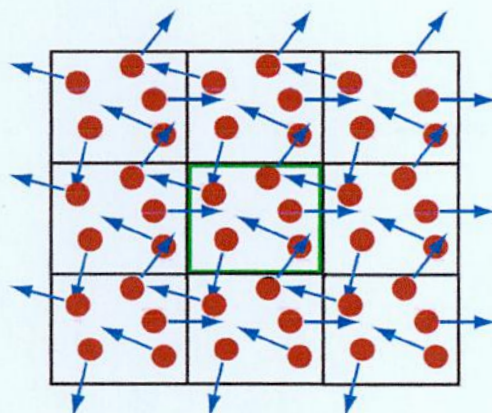
Figure 2.9: Graphical representation of the periodic boundary conditions of the middle box. The arrows indicate the velocities of atoms. The atoms in the middle box can interact with atoms in the neighboring boxes without having any boundary effects.

2.4. LAMMPS Package

LAMMPS (Large-scale Atomic/Molecular Massively Parallel Simulator) is a molecular dynamics program from Sandia National Laboratories [87, 88]. It is used to perform the molecular dynamics simulation. LAMMPS can model atomic, polymeric, biological, metallic, granular, and coarse grained systems using a variety of force fields and boundary conditions. LAMMPS can model systems from a few particles up to million or billions.

2.4.1 MD Simulation Technique using LAMMPS
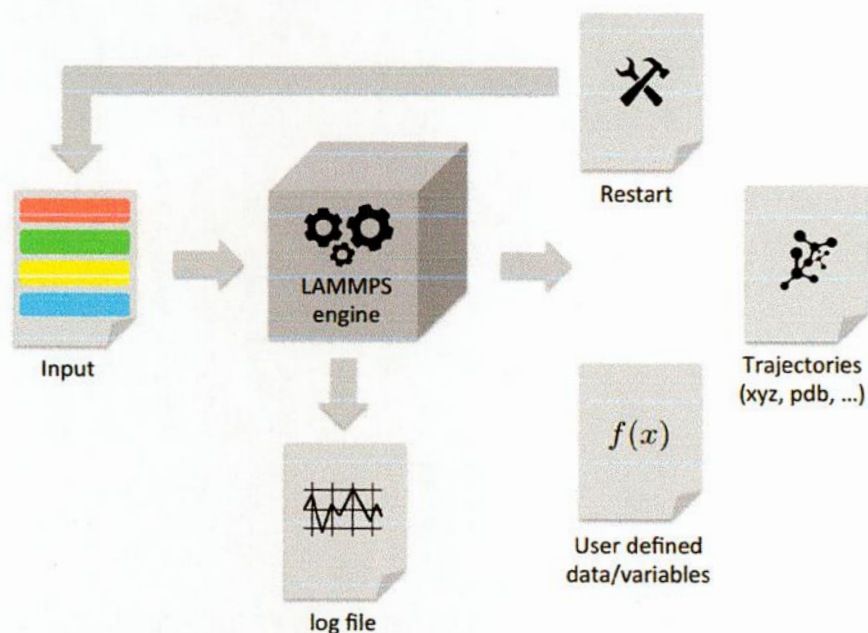
Figure 2.10: Graphical representation of the MD simulation technique using LAMMPS.

2.4.2 LAMMPS Input-file Overall Structure
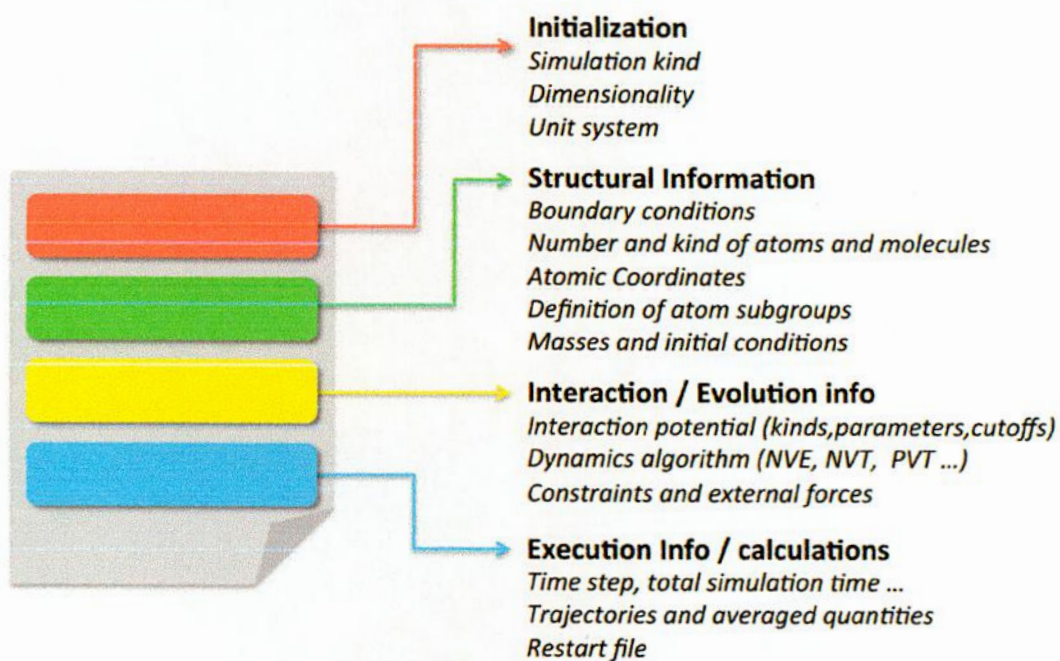
Figure 2.11: Structure of the input file of LAMMPS.

2.4.3 Output-(.log-file) Overall Structure
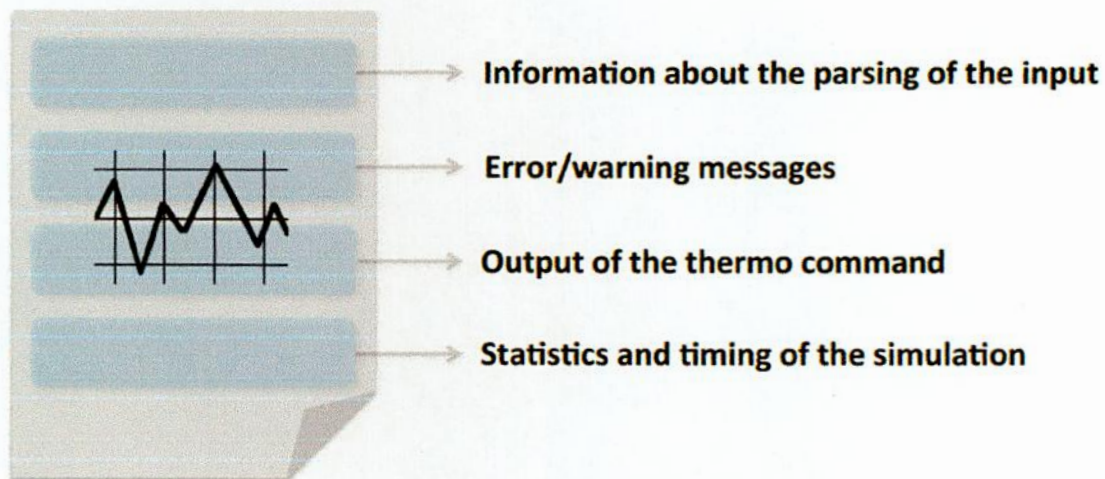
Figure 2.12: Structure of the output file of LAMMPS.

2.4.4 Computations and Output
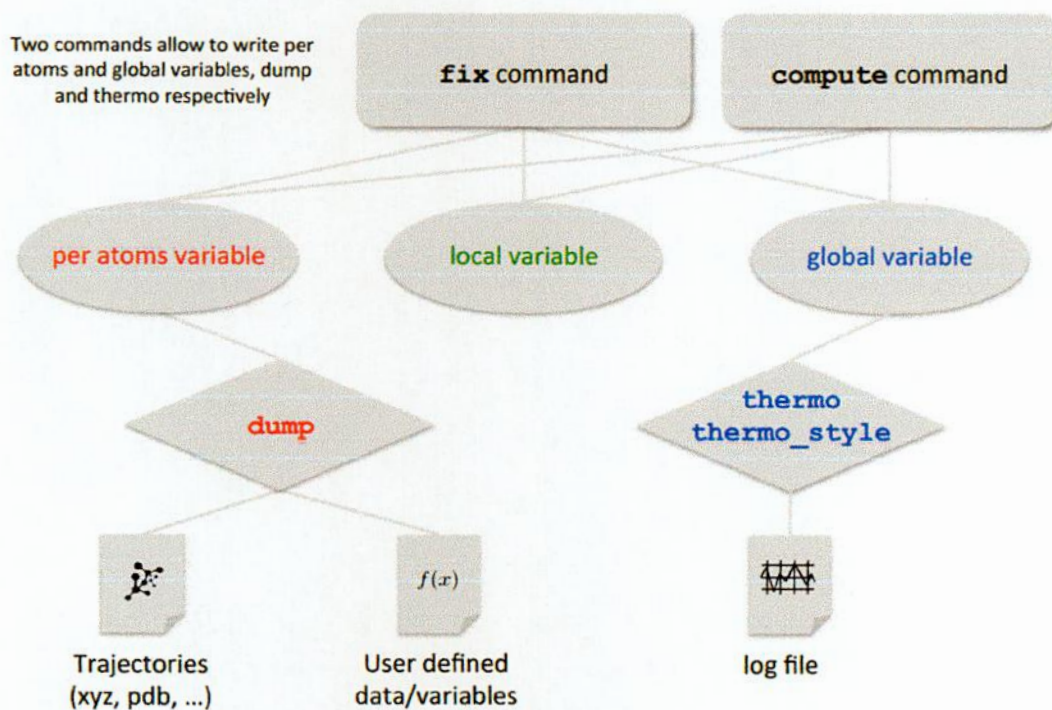
Figure 2.13: Output file generation in LAMMPS.

```
fix                         1 all nve
fix                         hot all heat 1 100.0 region hot
fix                         cold all heat 1 -100.0 region cold
thermo_style                custom step temp c_Thot c_Tcold
thermo                      1000
run                         10000
# thermal conductivity calculation
compute                     ke all ke/atom
variable                    temp atom c_ke/1.5
compute                     layers all chunk/atom bin/1d z lower 0.05 units reduced
fix                         ave/chunk 10 100 1000 layers v_temp file profile.heat
variable                    tdiff equal f_2[11][3]-f_2[1][3]
fix                         ave all ave/time 1 1 1000 v_tdiff ave running start 13000
thermo_style                custom step temp c_Thot c_Tcold v_tdiff f_ave
run                         20000
```

2.5 OVITO Package

Open Visualization Tool (OVITO) is a molecular visualization program [89] for displaying, animating, and analyzing large bio-molecular/material systems using 3-D graphics and built-in scripting. It supports all computer platforms, processors and not limited by no of particles in the system under observation except available computational memory. It is distributed as open-source software and can be downloaded from the website http://ovito.sourceforge.net/. Figure 2.14 shows a typical screenshot of the main window of OVITO.
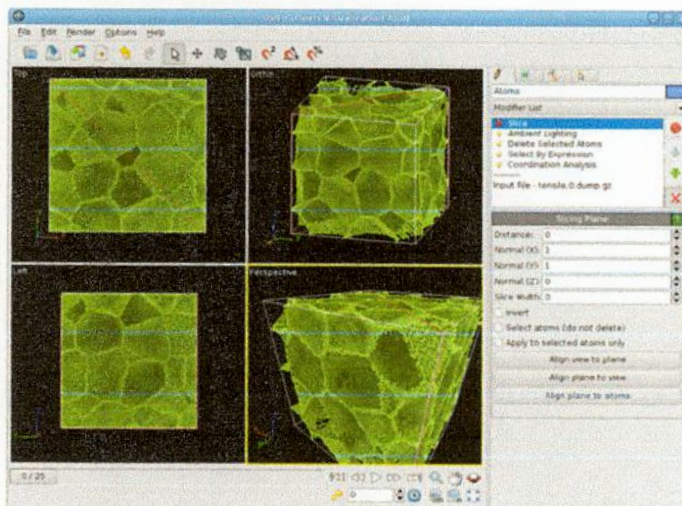
Figure 2.14: Screenshot of the main window of OVITO.

CHAPTER III

Computational Details

3.1 Introduction

In molecular dynamics simulation, equilibrium molecular dynamics (EMD) and non-equilibrium molecular dynamics (NEMD) are two techniques by which thermal conductivity of materials can be calculated. Each of them has their own advantages and disadvantages. The EMD based on the Green-Kubo method needs very high computational cost to converge the heat current autocorrelation factor (HCACF) to calculate the thermal conductivity of a large sheet. However, the non-equilibrium MD based on Fourier's law is very simple and needs a lower computational cost than EMD to calculate the thermal conductivity of a large sheet. Therefore, NEMD simulation [90] especially the 'heat flux control' or 'reverse' technique is used here to calculate the thermal conductivity of the 2D-SiC sheet. In this chapter, a detailed description about the reverse non-equilibrium molecular dynamics simulation technique is given. The Fourier transform of the velocity auto-correlation of atoms for the phonon density of states calculation and the procedure for quantum correction of thermal conductivity at low temperature range are also provided here. In addition, for the calculation of mechanical behavior of 2D-SiC, the virial stress theorem is also discussed here in details.
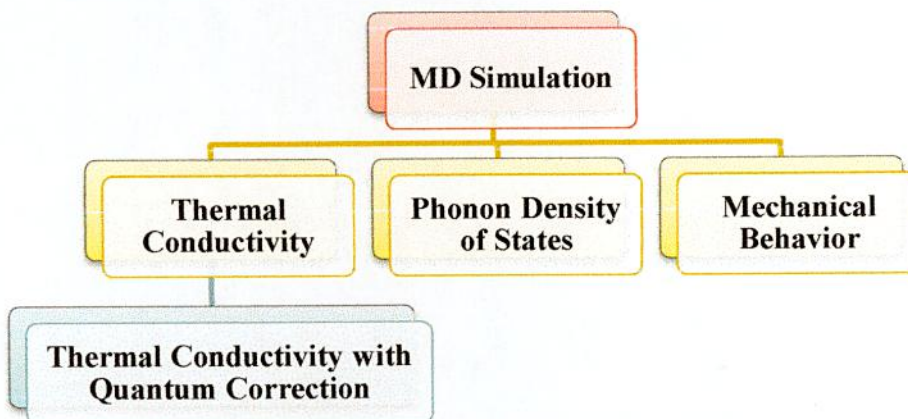
Figure 3.1: Calculation of different properties of 2D-SiC using Molecular Dynamics (MD) Simulation.

3.2 Reverse Non-equilibrium Molecular Dynamics (RNEMD) Simulation

The RNEMD is a "Direct Approach" in which the thermal conductivity is calculated by imposing the 'heat flux' as the system input and measuring 'temperature gradient' as the system output with the help of Fourier's law as follows [90]:

$$k_x = -\frac{J_x}{dT/dx} \tag{3.1}$$

where J_x is the 'heat flux' (system input), dT/dx is the 'temperature gradient' (system response), and k_x is the thermal conductivity along the X direction.

Temperature gradient along the computational direction (X) is computed by dividing the whole nanosheet into N slab. Then at a distance of '$X/4$' a 'hot slab' and '$3X/4$' a 'cold slab' is made by imposing a small amount of heat ΔQ in the 'hot slab' and removing $-\Delta Q$ amount of heat from the 'cold slab' at every time step. Velocity rescaling process for kinetic energy modification of atoms is applied in both the 'hot slab' and 'cold slab' for the creation of temperature gradient between them. As the total energy is conserved in this procedure, there occurs a temperature gradient due to the energy swap from the 'hot slab' to the 'cold slab'. Reaching to the steady state condition, as the swap heat energy ΔQ in the 'hot slab' has an equal magnitude of $-\Delta Q$ in the 'cold slab' it can be written that,

$$|\Delta Q| = |\Delta Q'| = \Delta\varepsilon = \frac{1}{2}\Sigma_{transfer}\frac{m}{2}(v_{hot}^2 - v_{cold}^2) \tag{3.2}$$

Again from the definition of heat flux, the J_x can be rewritten,

$$J_x = \frac{\Delta\varepsilon}{AMt} = \frac{1}{2MAt}\Sigma_{transfer}\frac{m}{2}(v_{hot}^2 - v_{cold}^2) \tag{3.3}$$

where, J_x represent the imposed heat flux, $\Delta\varepsilon$ represents the kinetic energy difference between hottest and coldest atoms in every M time steps (M is known as heat energy exchange frequency), t represents the MD time step, m, v_{hot} and v_{cold} represents the atomic mass, lowest velocity atoms in the 'hot slab' and highest velocity atom in the 'cold slab', respectively and A represents the cross-sectional area which is equal to wh. In the equation, the $1/2$ factor is taken due to the periodicity of the system that means heat energy can be passed in both directions.

Moreover, before the calculation of temperature gradient of the whole sheet, it is necessary to find out the temperature of each slab that depends on the velocities of atoms in that particular slab. The temperature of each slab is calculated as follows [91].

$$T_p = \frac{1}{3N_p k_B} \sum_{q=1}^{N_p} m_q v_q^2 \tag{3.4}$$

where, N_p denotes the number of atoms in slab p, k_B represents the Boltzmann constant, m_q, and v_q represents the mass and velocity of atom q in the slab.

Furthermore, before applying the heat flux in the system, the system is first equilibrated at desired temperature. To remove the size effects, periodic boundary conditions are applied along the X and Y directions of the SiC sheet. Conjugated Gradient Algorithm (CGA) was used for energy minimization of the structures. After energy minimization, constant number of atoms, pressure and temperature (*NPT*) ensemble MD simulation for 10^5 time steps were performed to switch the system to the target temperature and pressure with a time step of 0.5 fs. Velocity-verlet integration technique was applied to achieve the desired temperature with a Gaussian distribution. Here, constant number of atoms, volume and energy (*NVE*) ensemble integration is then applied for 10^5 time steps for temperature rise from initial temperature to the desired temperature. Furthermore, 2×10^5 time steps of *NPT* integration are performed to stabilize the temperature and pressure. Moreover, another 3×10^5 time steps *NVE* ensemble MD simulation was performed to conserve the energy and volume of the system. Thus, the system is equilibrated and the system is ready for passing the heat flux at desired temperature. After equilibration, a small amount of heat energy is applied into 'hot slab' and same amount of heat energy is removed from the 'cold slab' with *NVE* ensemble integration technique. Here the *NVE* ensemble with Nose-Hoover thermal bath is used for 5×10^5 time steps for achieving equilibration with ensuring that the energy is conserved and the heat is transported from the hot 'slab' to the 'cold slab' to attain steady state. Then another 12×10^6 time steps run is allowed to attain the time-averaged temperature profile of the sheet, which is used to calculate the temperature gradient *dT/dx*.
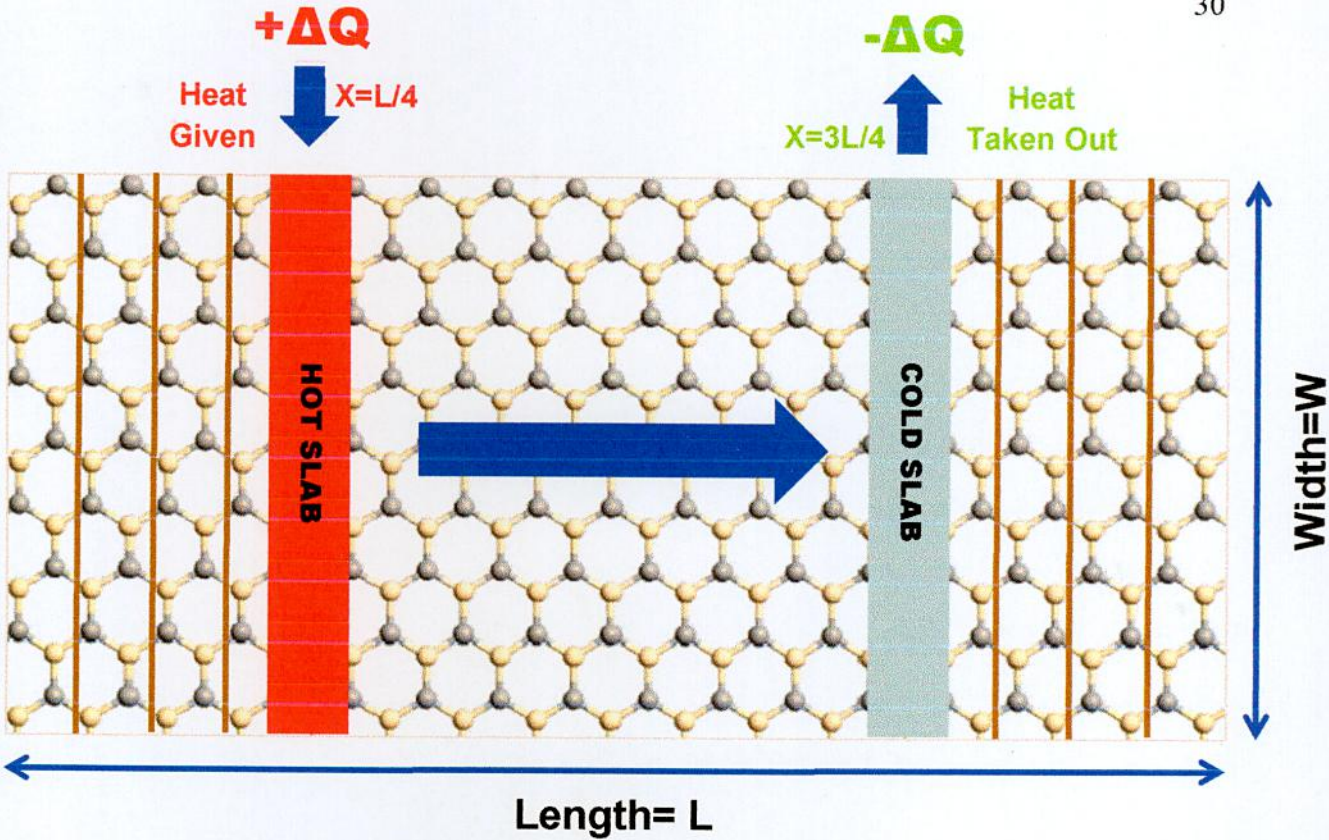
Figure 3.2: 2D-SiC sheet for thermal conductivity calculation using Reverse Non-equilibrium Molecular Dynamics Simulation (RNEMD).

After achieving steady state condition, Fourier's law of heat conduction is used to calculate the thermal conductivity of the 2D-SiC sheet as follows,

$$k_x = -\frac{\frac{1}{2AMt}\sum_{transfer}\frac{m}{2}(v_{hot}^2 - v_{cold}^2)}{dT/dx} \tag{3.5}$$

In the simulation, the width of the SiC sheet was kept at 10 nm with thickness of 3.50 Å. The direction of heat flux is X and heat exchange frequency M is set at 1000. Furthermore, in molecular dynamics simulation, the nanosheet or bulk material property is largely depended on the classical interatomic potential. In this works, optimized tersoff potential proposed by *Albe et al.* [92] as well as original tersoff potential [93] are used to study the impact of these classical potentials on the thermal conductivity of 2D-SiC. Though, recently 2D materials such as graphene and carbon nanotubes (CNTs) systems used reactive empirical bond-order (REBO) and

adaptive intermolecular reactive empirical bond order (AIREBO) potential to analyze the thermal and mechanical properties, it has been reported that, analytical potential proposed by Albe *at al.* can perfectly reproduce the experimental results of dispersion curves and phonon mode group velocities of the 2D-SiC system.

3.3 Phonon Density of States Calculation

To quantify the length and temperature dependent thermal conductivity, the phonon density of states (PDOS) of 2D-SiC is calculated at different temperature and length. The phonon density
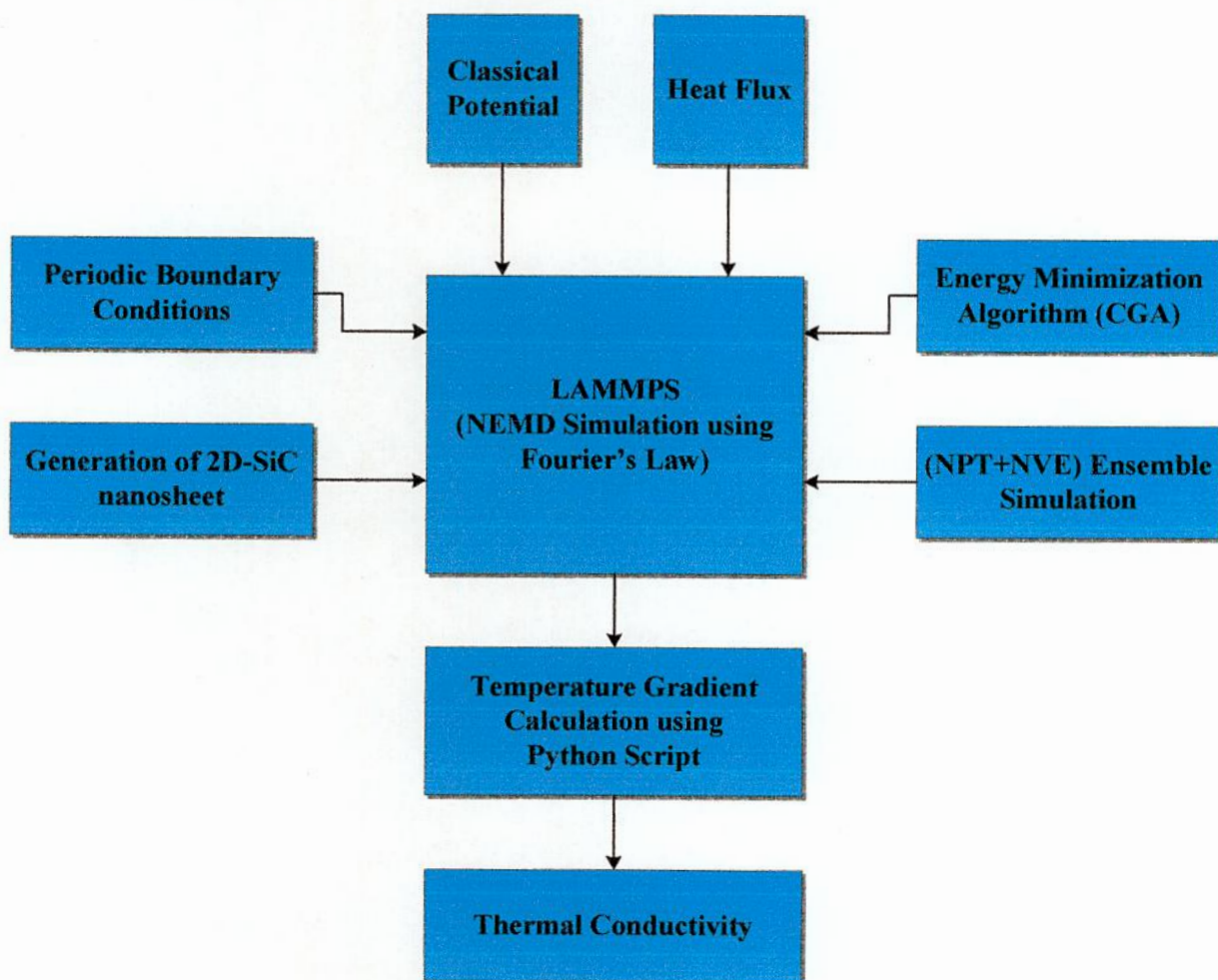
Figure 3.3: Basic block diagram for thermal conductivity calculation using Non-equilibrium molecular dynamics (NEMD) simulation in LAMMPS.

of states was obtained from the Fourier transforms of the velocity auto-correlation function defined as [94]:

$$Z_\alpha(t) = \frac{<V_{i\alpha}(0)\cdot V_{i\alpha}(t)>}{<V_{i\alpha}(0)\cdot V_{i\alpha}(0)>} \quad (3.6)$$

where, $v_{i\alpha}$ (t) and $v_{i\alpha}$ (0) represents the velocity of the ith particle of species α (Si or C) at time t and time 0, respectively and the brackets denote averages over atoms and time origins.

Finally, the phonon density of states is found by the formula of

$$F(\omega) = \sum_\alpha F_\alpha(\omega) \quad (3.7)$$

where, $F(\omega)$ denotes the phonon spectrum, ω is the vibrational wavenumber and $F_\alpha(\omega)$ is the partial phonon density of states which can be represented as, $F_\alpha(\omega) = \frac{6N_\alpha}{\pi} \int_0^\infty Z_\alpha(t) \cos(\omega t)\, dt$.

3.4 Quantum Correction

The classical molecular dynamics (MD) simulation is the most popular technique which can be used to predict the thermal properties of 2D materials efficiently at different sets of condition. The MD simulation is considered valid near and above a material's Debye temperature, where all of the vibrational (*i:e:*, phonon) modes are fully excited. However, it cannot predict the thermal conductivity at lower temperature ranges where quantum effects are significant, i.e. majority of the phonon modes reside in their ground state. As 2D-SiC is expected to be applied in nanoelectronics as well as optoelectronics applications with different temperature ranges, it is also important to explore its low temperature thermal conductivity using the quantum correction.

If one knew the contributions of the phonon density of states (PDOS) as a function of phonon frequency, it is possible to obtain the quantum correction with the help of phonon/normal mode specific heat capacities that calculates the reduced contributions for the many modes that are not fully excited, thereby resulting in a reduced thermal conductivity. At the lower temperature range, the quantum corrected thermal conductivity can be calculated with the help of specific heat capacity at constant volume defined by [94],

$$C_V = \frac{3Nk_B \int_0^\infty \frac{u^2 e^u}{(e^u-1)^2} F(\omega)d\omega}{\int_0^\infty F(\omega)d\omega} \quad (3.8)$$

where, k_B Is the Boltzmann Constant and $u = \frac{\hbar\omega}{k_B T}$. The Debye temperature Θ_D can be approximated from the equation of $C_V = \frac{12}{5}\pi^4 N k_B (\frac{T}{\Theta_D})^3$.

Finally, the quantum corrected thermal conductivity is calculated using the relation of

$$k_{corrected} = (\frac{C_v}{3Nk_B}) \times k_{MD} \qquad (3.9)$$
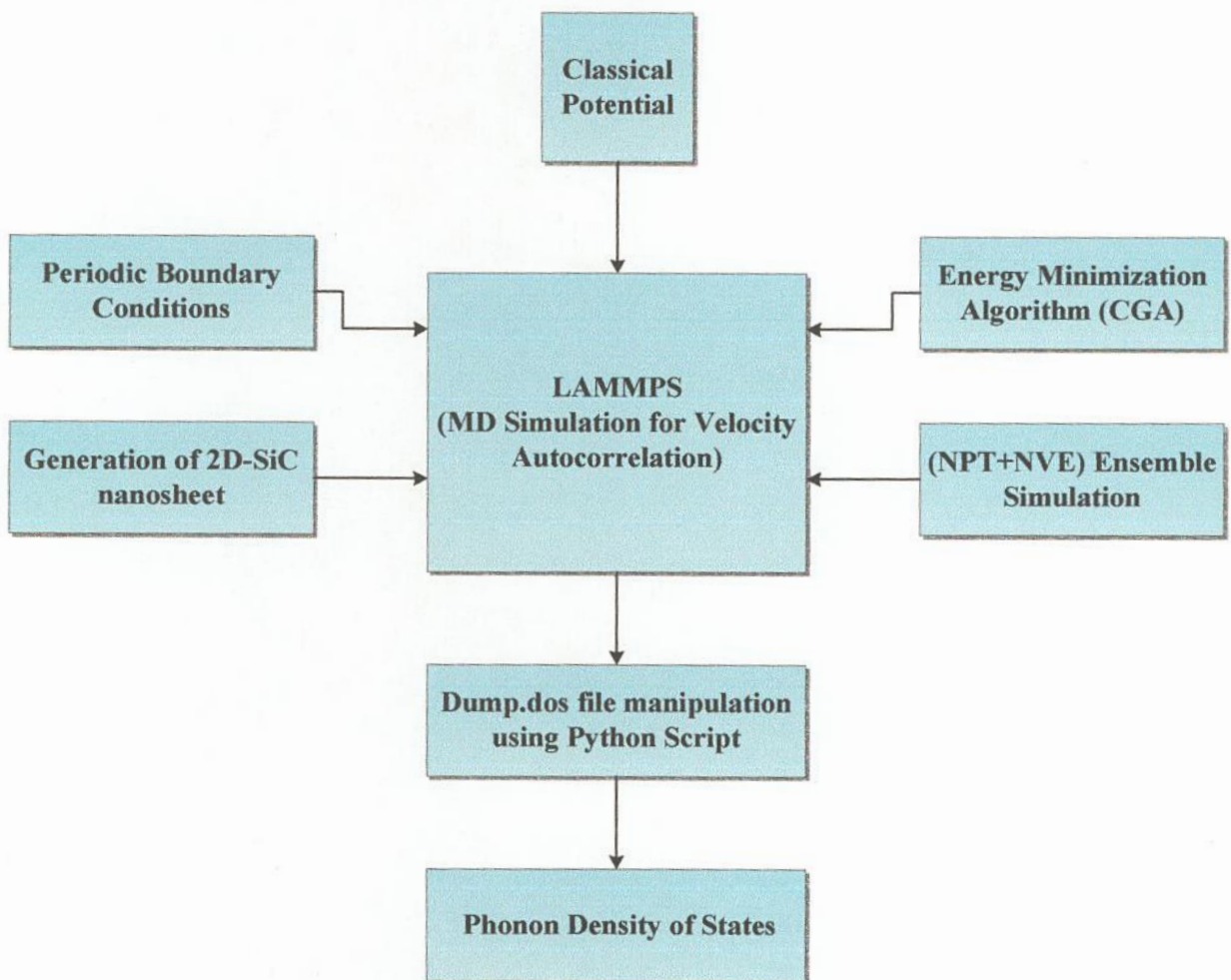
Figure 3.4: Basic block diagram for the phonon density of states calculation using molecular dynamics (MD) simulation in LAMMPS.

3.5 Mechanical Behavior Characterization using Molecular Dynamics Simulation

To calculate the mechanical behavior of 2D-SiC sheet, classical MD simulation is performed in the large-scale atomic/molecular massively parallel simulator (LAMMPS) package [87]. In MD simulation, accurate prediction of system properties largely depends on the classical interatomic potential employed in the simulation. In this work, classical Vashishta potential [94] is used to describe the atomistic interaction of 2D-SiC sheet containing different types of vacancy defects. This potential is validated by comparing the physical quantities with the experimental results. Although, interatomic potential proposed by several authors, e.g. Tersoff *et al.* [93], Tang *et al.* [95], Li *et al.* [96], Porter *et al.* [97], Noreyian *et al.* [98], Pearson *et al.* [99], Huang *et al.* [100] and Erhart and Albe *et al.* [92] to describe the elastic and thermal properties of SiC systems with defects, classical Vashishta potential proposed by Priya Vashishta *et al.* [94] opens a new insights for the SiC systems for defected case which is examined by density functional theory based first principle calculations. This potential has numerous features such as two-body as well as three-body covalent interactions, charge induced dipole-interactions due to electronic polarizations of ions, and induced dipole-dipole or Vander Waals interactions. For 2D-SiC systems, the two-body interactions are used to describe the steric repulsion as well as coulomb interactions. However, this is not sufficient to illustrate the effects of bond bending and stretching, and thus, three body interactions is used to describe the covalent interactions of Si-C-Si and C-Si-C like bonding.

To characterize the mechanical behavior, a sheet of length 30 nm and width 10 nm containing the total of 7524 atoms is used. Before applying the uniaxial loading along the length direction (X) of the 2D-SiC sheet, Conjugate Gradient Algorithm (CGA) is used for energy minimization of the system. The sheet is then allowed to relax over 20 ps with time step of 1 fs. A constant engineering strain of 10^9 s^{-1} is used as the strain rate to deform the sheet. Furthermore, Nose-Hoover thermostat-barostat *(NPT)* ensemble is used in the simulation to make the zero stress condition along the *Y* and *Z* direction of the simulation box to ensure uniaxial strain condition. Moreover, to remove the undesired oscillations during simulation; a damping constant of 1.0 is used in the *NPT* ensemble simulation. In MD simulation, the Cauchy stress [95] or the Virial stress [102] can be used to calculate strain-stress response. Although the Cauchy stress is computationally more efficient than the Virial stress, the initial nonzero physical

stress of the Cauchy stress model at high temperature condition hinders its applicability in the MD simulation. Thus, in this work, Virial stress theorem is used to calculate the mechanical behavior of 2D-SiC sheet. In MD simulation, the strain ε under tension can be described as follows,

$$\varepsilon = \frac{L-L_0}{L_0} = \frac{\Delta L}{L_0} \tag{3.10}$$

where, L_0 and L represent the lengths of the SiC nanosheet before and after tensile loading. Here L_0 is taken as the maximum length of the SiC nanosheet among various energy minimum states.

Now, the pressure of the system is computed by the formula of

$$P = \frac{Nk_BT}{V} + \frac{\sum_i^{N'} r_i \cdot f_i}{dV} \tag{3.11}$$

where N denotes the number of atoms in the nanosheet, k_B represents the Boltzmann constant, system temperature is denoted by T, d represents the dimensionality of the system (2 or 3 for 2d/3d), and V represents the system volume (or area in 2d). The second part of the equation represents the Virial part, which is equal to $-dU/dV$ and it is computed for all pairwise as well as 2/3/4/many-body, and long-range interactions, where r_i and f_i represents the position and force vector of the ith atom, and the black dot denotes a dot product between r_i and f_i. Figure 3.5 shows the monolayer SiC sheet for the characterization of mechanical behavior.
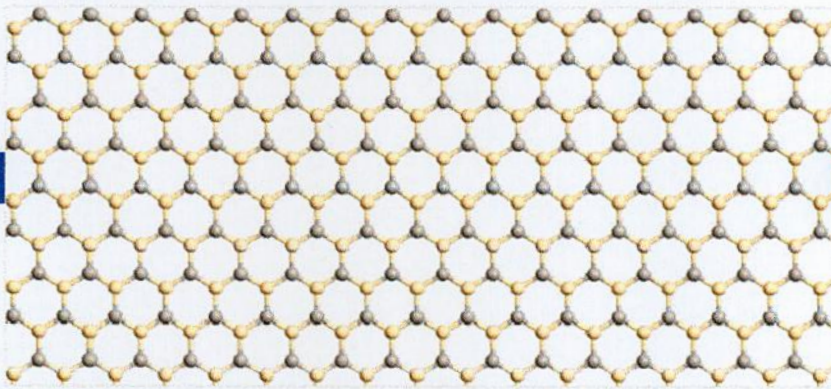
Figure 3.5: 2D-SiC sheet subjected to the uniaxial tensile strain.

In the stress calculation, when periodic boundary conditions are applied, the N' terms necessarily include periodic image (ghost) atoms outside the central box, and the r_i and f_i of the ghost atoms are thus included in the summation. However, when periodic boundary conditions are not applied, $N' = N =$ the number of atoms in the system. To obtain the stress–strain relations during tensile loading, the Virial stress P_{IJ} is calculated according to the equation of,

$$P_{IJ} = \frac{\sum_k^N m_k v_{kI} v_{kJ}}{V} + \frac{\sum_k^{N'} r_{kI} f_{kJ}}{V} \tag{3.12}$$

where N denotes the number of atoms in the system, V is the system volume, V_{kI} is the ith
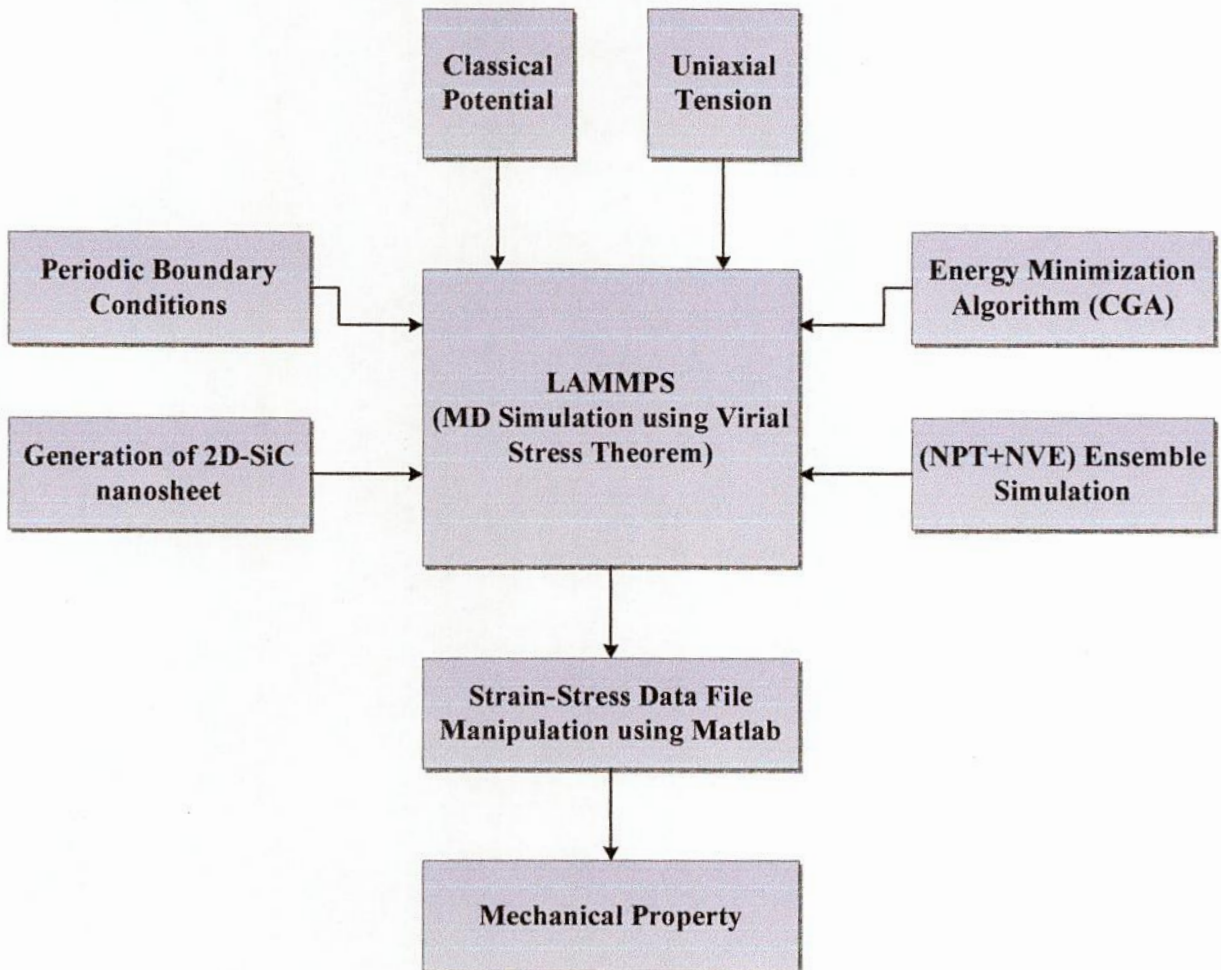
Figure 3.6: Basic block diagram for mechanical property calculation using molecular dynamics (MD) simulation in LAMMPS.

component of the velocity, r_{kl} is position of the kth atom and f_{kJ} is the jth component of the force which is applied on the kth *atom*. This equation of strain-stress calculation contains a kinetic energy (temperature) term and the Virial term (as the sum of pair, bond, angle, dihedral, improper and kspace terms).

The elastic modulus, E, of the 2D-SiC sheet can be calculated by using the following equation [103]:

$$E = \frac{1}{At}\frac{\partial^2 U}{\partial^2 \varepsilon}$$
(3.13)

where U and A represent the strain energy and surface area of the structure, respectively, and t denotes the thickness of the 2D-SiC sheet. Moreover, elastic modulus can also be attained by manipulating the slope of the linear part (at low strain levels) of stress-strain response, which also yields adequately the same result as that of Eq. (3.13) [103]. Besides, to visualize the trajectories of the strain-stress MD simulation OVITO package is used in this work.

CHAPTER IV

Results and Discussion

4.1 Introduction

This chapter provides the important new findings of 2D-SiC nanomaterial including its thermal, mechanical and phonon properties. The length and temperature dependent thermal conductivity of the 2D-SiC with a corresponding phonon density of states variation are given in details. Furthermore, the effects of quantum correction and interatomic potential on the thermal conductivity of 2D-SiC are also discovered. Finally, the mechanical behaviors such as tensile strength and elastic modulus of both the pristine and vacancy defected 2D-SiC at different temperature and vacancy concentration are explored.

4.2 Thermal Conductivity

4.2.1 Effect of System Length

Firstly, the length dependent thermal conductivity is explored considering a series of 2D SiC sheets having a uniform width of 10 nm but the length in the longitudinal direction is varied over a range from 10 nm to 600 nm. The considered 2D-SiC sheet is shown in Fig. 4.1. The maximum number of atoms considered in this simulation is 154800. The considered width (10 nm) is large enough to eliminate the size effects. Moreover, a sufficiently long simulation time is set to reach the steady state condition of the temperature gradient. Fig. 4.2 shows the temperature gradient profiles of 2D-SiC sheet at different simulation times. All the temperature gradient profiles exhibit linear behavior at steady state conditions. The linear temperature gradients yield thermal conductivity might be less erroneous.

The variation of thermal conductivity as a function of sheet length at room temperature is depicted in Fig. 4.3. It is noticeable that the thermal conductivity of 2D-SiC increases with the increase of sheet length. A thermal conductivity of 271.03 W/mK is obtained at the length 600 nm which is one order higher than that of silicene for the same length [115, 116]. 2D SiC exhibits a planar structure whereas silicene posseses buckling configuration which is one of the possible
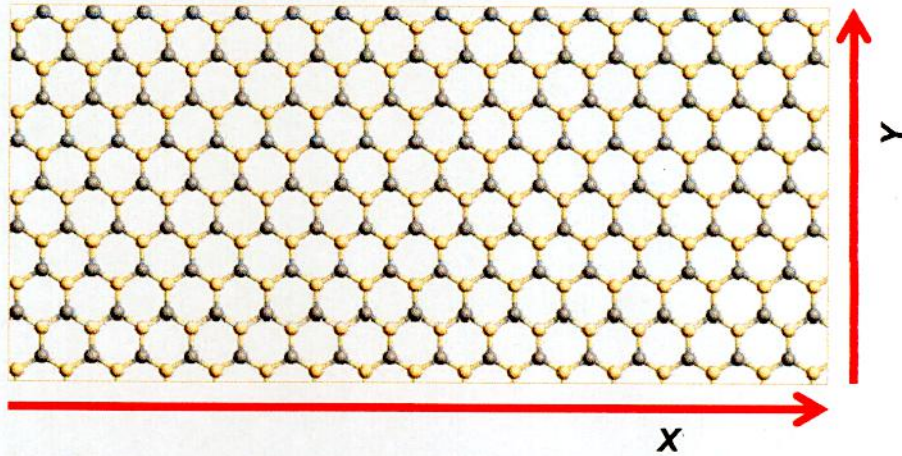
Figure 4.1: Monolayer 2D-SiC sheet for thermal conductivity calculation.
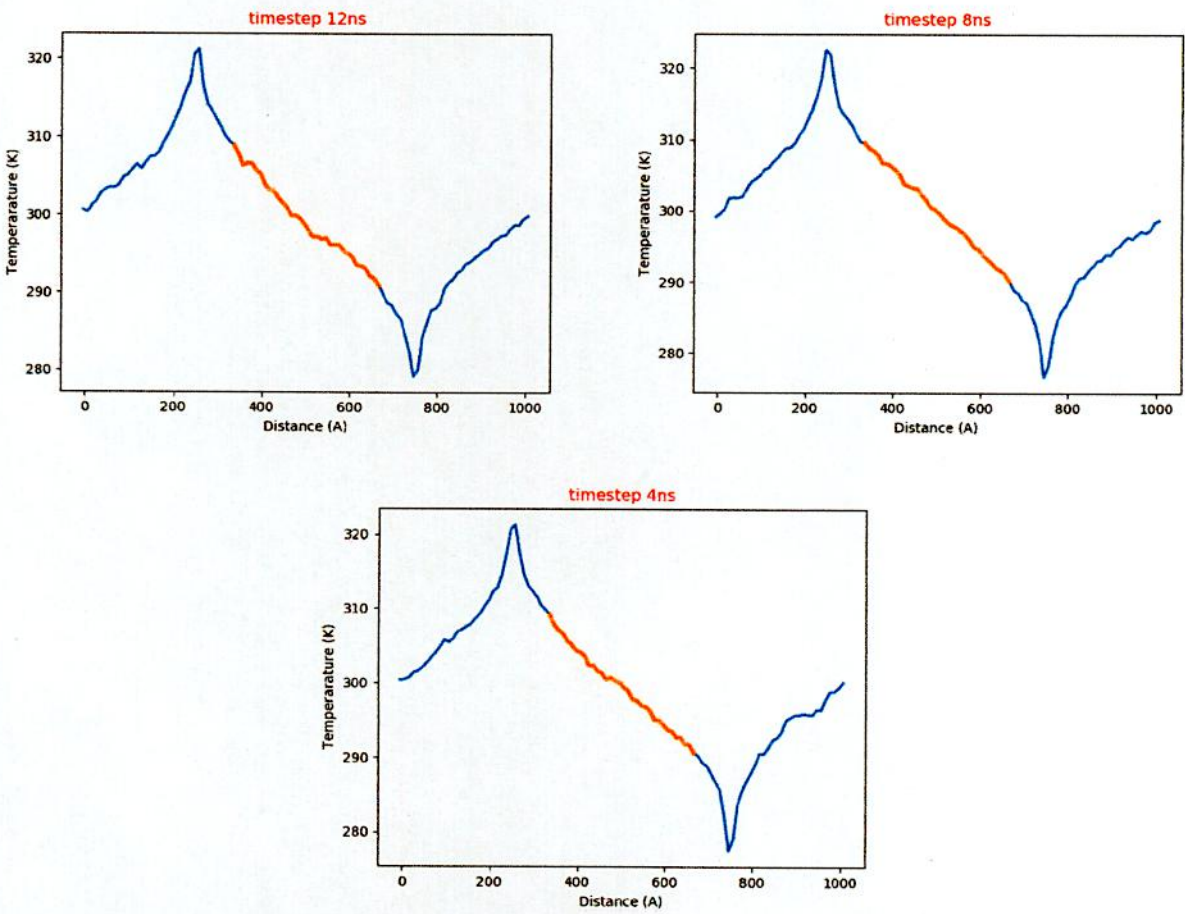
Figure 4.2: Steady state temperature gradient profiles along the computational direction for different simulation times.

reasons for this higher value. Again, the Debye temperature and phonon group velocities [54] of 2D-SiC may also responsible for this higher value of thermal conductivity of 2D-SiC compared to silicene. In contrast, the obtained value of thermal conductivity is much smaller than that of graphene [55]. It is important to note that graphene is a single component system of C atoms whereas 2D-SiC is a binary system of Si and C atoms which leads to additional phonon-phonon scattering mechanism. In this context, recently Che *et al.*[109] reported ~37% drop of the thermal conductivity in a binary system compared to a single component system.
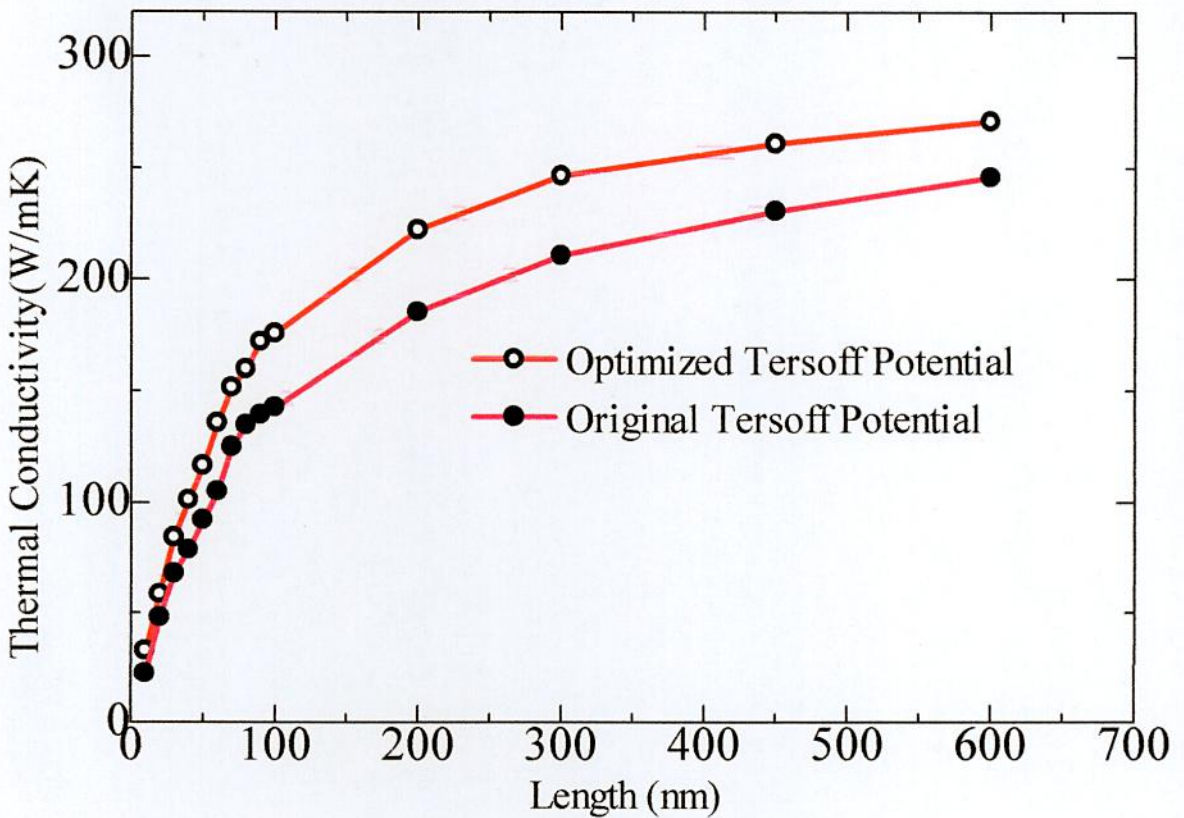
Figure 4.3: Length dependent thermal conductivity of 2D-SiC using original and optimized tersoff potential

4.2.2 Effect of Interatomic Potential

In molecular dynamics simulation, it is important to choose a proper interatomic potential in order to interpret the atomistic interaction appropriately. Hence, the thermal conductivity of the present work is calculated using two classical potentials: original tersoff potential and optimized tersoff potential. It is found that NEMD simulation using original tersoff potential gives a lower value of thermal conductivity rather the optimized tersoff potential for different length and temperature. This attributes to the variation in phonon group velocity and phonon dispersion energy of 2D-SiC produced by these two classical potentials. According to Albe *et al.* [92], the original tersoff potential cannot produce the exact phonon dispersion curve. Instead, it underestimates the thermal conductivity due to the inappropriate measures of acoustic mode group velocities and phonon-phonon scattering rate near zone center. It also underestimates the out of plane acoustic mode phonon dispersion. In comparison, as reported by Albe *et al.* [92] optimized tersoff potential perfectly produces the phonon dispersion curve using an analytical model which is verified by density functional theory based first principles calculation. Therefore, the optimized tersoff potential yielded thermal conductivity estimation of 2D-SiC sheet is more accurate due to the reduced phonon-phonon scattering rate and improved approximation of acoustic phonon branches along with the proper fitting of near zone centers velocities.

4.2.3 Effect of Temperature

In order to investigate the effect of temperature on the thermal conductivity, a temperature range of 100 K to 700 K is considered in this work with a SiC sheet of 100 nm in length and 10 nm in width. The change of the thermal conductivity of 2D-SiC sheet with respect to temperature is illustrated in Fig. 4.4. A decreasing behavior of the thermal conductivity is observed with respect to temperature both for original and optimized tersoff potential. At 100 K temperature, the optimized tersoff potential yields a thermal conductivity of 297.14 W/mK for 2D-SiC whereas it was 227.24 W/mK for original tersoff potential. For 2D-SiC, above room temperature, it is observed that the thermal conductivity deviates the normal *1/T* law and shows an anomalous slowly decreasing behavior for both optimized and original tersoff potential. This types of anomalous thermal conductivity reduction trend in this 2D-SiC may be occurred due to the mass variation of Si and C atoms as well as strong polarization effect between them.
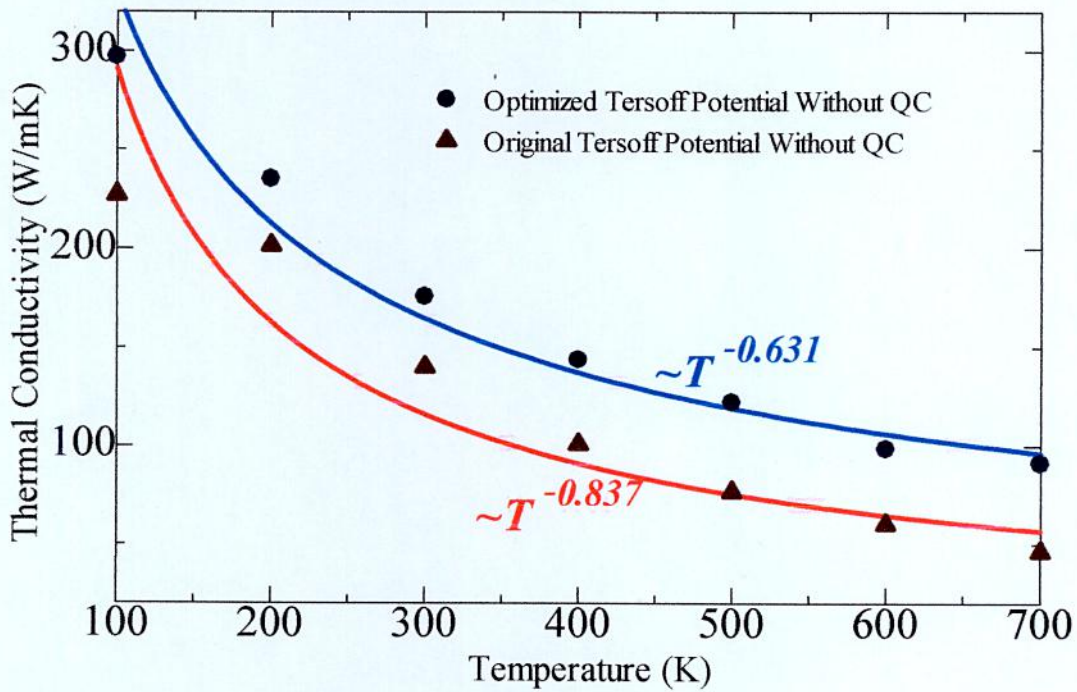
Figure 4.4: Temperature dependent thermal conductivity of 2D-SiC using optimized and original tersoff potential without quantum correction.

4.2.4 Phonon Density of States

In 2D materials, rather than the electron, the role of the phonon is more significant in heat transport [35]. The phonon scattering effect, the variation of phonon dispersion as well as the phonon density of states of 2D materials are quite different from their bulk crystal structure, which results in a variation of thermal conductivity with different geometry and environmental conditions [105-108]. Moreover, among the phonon modes in 2D materials, the acoustic phonons are the main heat carriers [55], which play a significant role in the heat transport compared to the optical phonons. With a view to elucidating the heat transport phenomena quantitatively at different length and temperature conditions, the acoustic phonon density of states are investigated.

The estimated velocity auto-correlation function for both the C and Si atoms is shown in Fig. 4.5 and Fig. 4.6, respectively. The velocity auto-correlation function shows a diminishing behavior for a correlation period of 3.5 ps due to an interaction between the atoms as well as arbitrary forces from neighboring atoms, inhibiting an epitome oscillatory motion. If there is no dealings, then the initial oscillation will upshots for all correlation periods. The phonon density of states is thus calculated from this VACF.
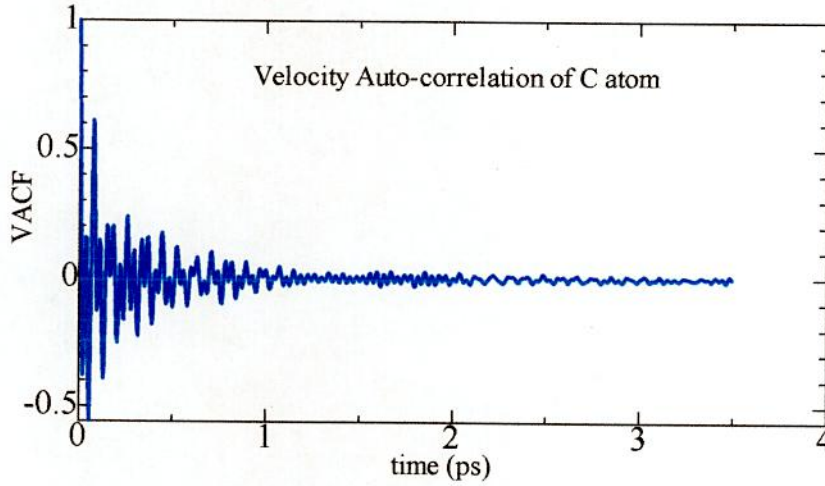
Figure 4.5: Velocity Auto-correlation Function for C atom.
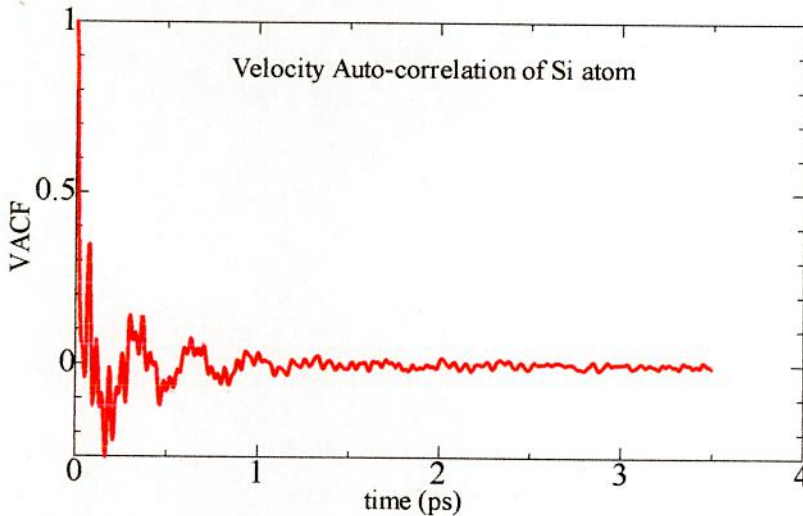
Figure 4.6: Velocity Auto-correlation Function for Si atom.

The phonon density of states of 2D-SiC for varying length is presented in Fig. 4.7. As the Fig. 4.7 suggests, with the increase of sheet length, a strengthened behavior is noticed in the peaks of the PDOS curve due to the increased availability of the low frequency acoustic mode phonons. In single layer graphene, based on the Klemens approximation [104], Nika *et al.* claimed that the contribution from flexural acoustic or out of plane acoustic (ZA) phonon is negligible due to its large Grüneisen parameter and small group velocity [57]. Meanwhile, Mingo *et al.* argued that ZA phonons carry most of the heat in graphene [64]. At low temperatures, the ZA modes is predicted to lead to a $\sim T^{1.5}$ behavior of the thermal conductivity, while the in-plane longitudinal acoustic (LA) and transverse acoustic (TA) phonons lead to a $\sim T^2$ behavior. In comparison, for binary compound such as 2D-GaN and 2D-ZnO, substantial contribution of the ZA mode phonons on the thermal transport up to 350 K temperature is reported [59, 60, 61]. Thus, it is predicted for 2D-SiC that the heat conduction at room temperature is due to the participation of all the low frequency LA, TA, and ZA mode phonons and their participations are increased
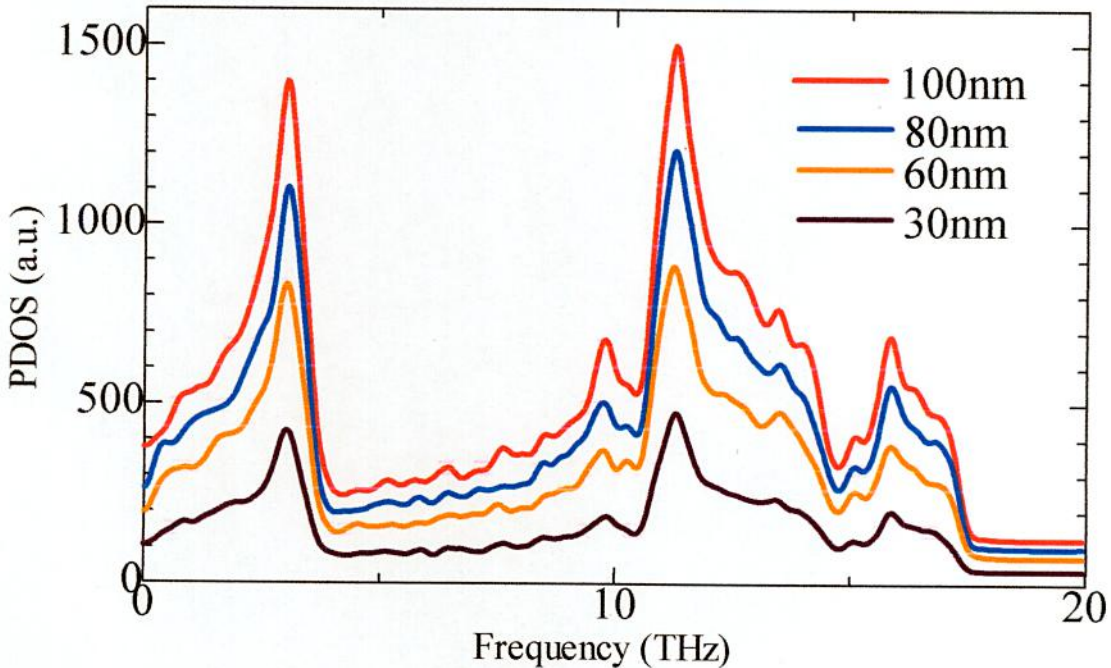
Figure 4.7: Length dependent acoustic phonon density of states of 2D-SiC using velocity autocorrelation of atoms at 300K temperature.

45

when the sheet length is increased. Moreover, from the PDOS curve it is observable that at room temperature, due to the negligible influence of the high frequency phonon modes, the peaks do not show any red shift or blue shift behavior. These may cause the increasing trend of thermal conductivity of 2D-SiC at increased sheet length.

Fig. 4.8 shows the temperature dependent PDOS curves for 2D-SiC. It is manifested that at high temperature, the peaks of the PDOS curve show decreasing nature with temperature. A blue shift is perceived from the first peak and a red shift is perceived from the second peak of the PDOS curve. Therefore, at higher temperature, due to the frequency shrinking and softening nature of the PDOS curves, a decreasing trend of the thermal conductivity of 2D-SiC is observed. However, the question is why slowly decreasing trend is observed in this 2D-SiC ? In binary systems, at higher temperature, a considerable influence of high frequency phonon modes as well as Umklapp limited phonon scattering are occurred [59, 60, 61]. With the increase of
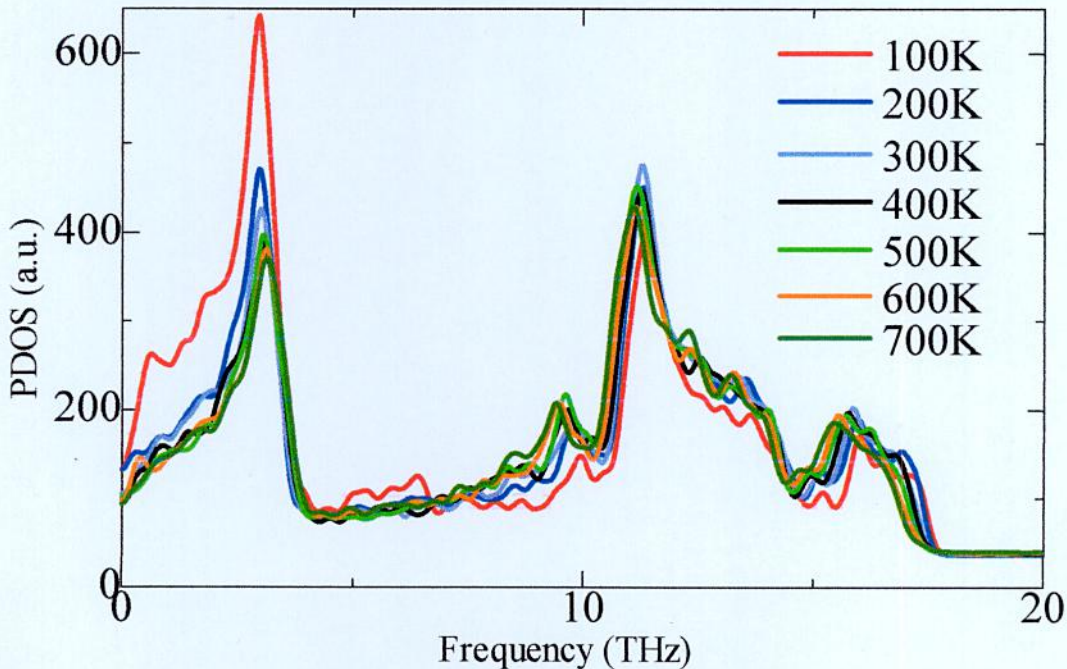
Figure 4.8: Temperature dependent acoustic phonon density of states of a 30 nm 2D-SiC sheet using velocity autocorrelation of atoms from 100 K to 700 K temperature.

temperature, the phonon-phonon scattering, specifically the Umklapp scattering is increased. Consequently, the PDOS curve shows a softening nature at high temperature region. What is more, due to the influence transfer from ZA modes phonon to high frequency longitudinal optic (LO) modes phonon, a blue shift along with red shift is observed in the PDOS results. Therefore, an anomalous decreasing trend of thermal conductivity is noticed in this binary 2D-SiC and it is reported that this type of phenomena is occurred due to the mass variation and electronegativity of binary systems [59, 60, 61]. Moreover, as Fig. 8 suggests, the PDOS of 2D-SiC is limited to 20 THz frequency range, whereas comparatively, the PDOS for graphene is reported as 50 THz to 60 THz [112-114] range. This discrepancy of PDOS range can be a reason for the smaller thermal conductivity of 2D-SiC with compared to graphene.

4.2.5 Quantum Corrected Thermal Conductivity

It is well known that thermal conductivity computation using MD simulation is not valid at low temperature due to the freezing effect of phonon modes. Therefore, Quantum corrections are necessary to study the low temperature thermal conductivity. To investigate the thermal conductivity of 2D-SiC at low temperature, the normal mode specific heat capacity have been calculated.
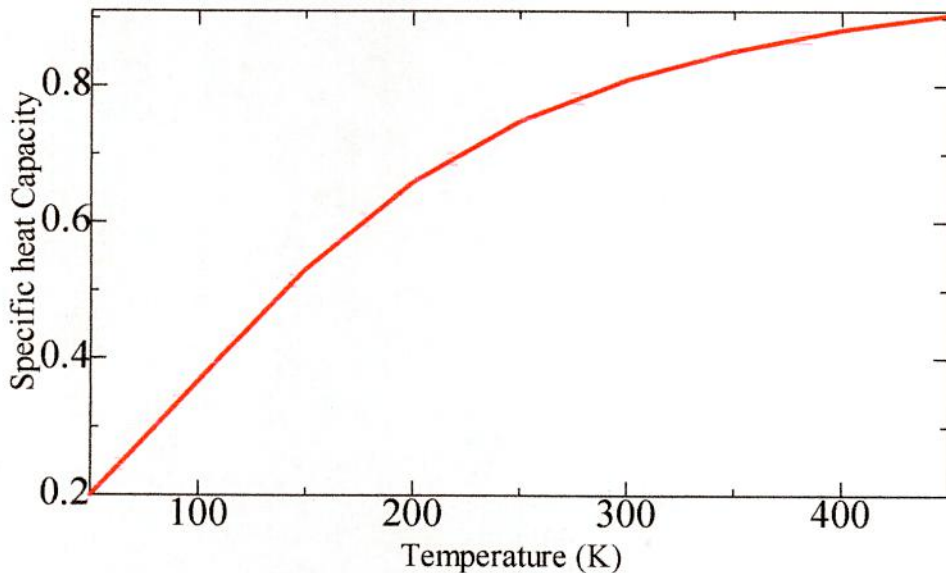
Figure 4.9: Specific heat capacity versus temperature.

The calculated specific heat capacity of a 2D-SiC sheet of 100 nm in length and 10 nm in width is shown in Fig. 4.9. With the increase of temperature, the phonon modes get excited and the specific heat capacity results a strengthened behavior. At higher temperature, the low frequency phonon modes are fully excited and the heat capacity goes into saturation.

Fig. 4.10 and Fig. 4.11 show the quantum corrected thermal conductivity of 2D-SiC for both optimized and original tersoff potential, respectively. Unlike, the un-corrected direct MD results, which monotonically decrease with temperature, the quantum corrected thermal conductivity shows an increasing trend up to Debye limit due to the rising behavior of the specific heat capacity. Moreover, it is explored that up to the Debye limit the thermal conductivity shows very small value compared to the thermal conductivity without quantum correction due to the lower number of excited phonon modes. Again up to quantum limit it is
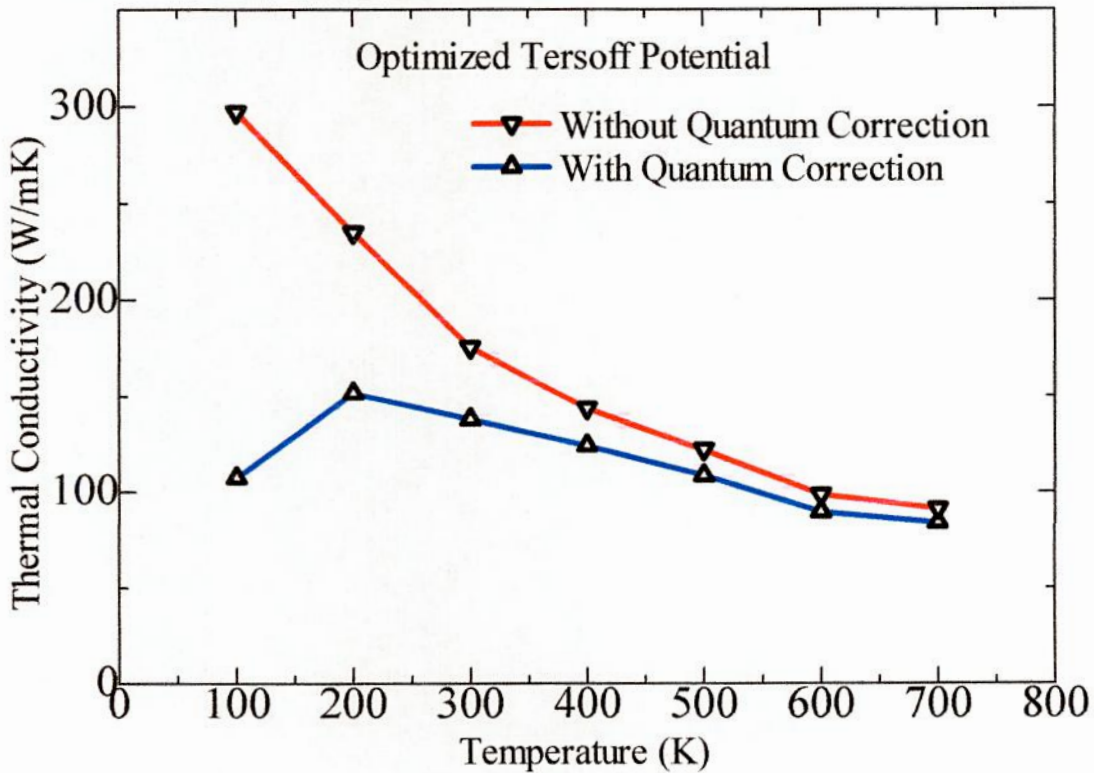
Figure 4.10: Temperature dependent thermal conductivity of 2D-SiC using optimized tersoff potential with and without quantum correction.

supposed that the group velocities of the phonons remain unchanged. At high temperature, above the quantum limit influences of the specific heat capacity on the thermal conductivity is supposed negligible due to its saturated nature [117] and effects of high frequency phonon modes and phonon anharmonicity are considered. Therefore, beyond 207 K temperature a decreasing trend of the thermal conductivity is noticed in the quantum corrected results.

The quantum corrected thermal conductivity nature of 2D-SiC at low temperature range can be explained with the help of PDOS results. For different binary systems it is reported that, up to room temperature, the ZA mode phonon is responsible for heat transport and with the increase of temperature it gradually losses its control [60, 61]. Near and above the room temperature, the LA and TA modes contribute a large than FA mode. From Fig. 4.12, it is found that up to room temperature the second and third peaks of the PDOS curve increase significantly, whereas the first peak shows a rapid decreasing behavior with temperature, which may be
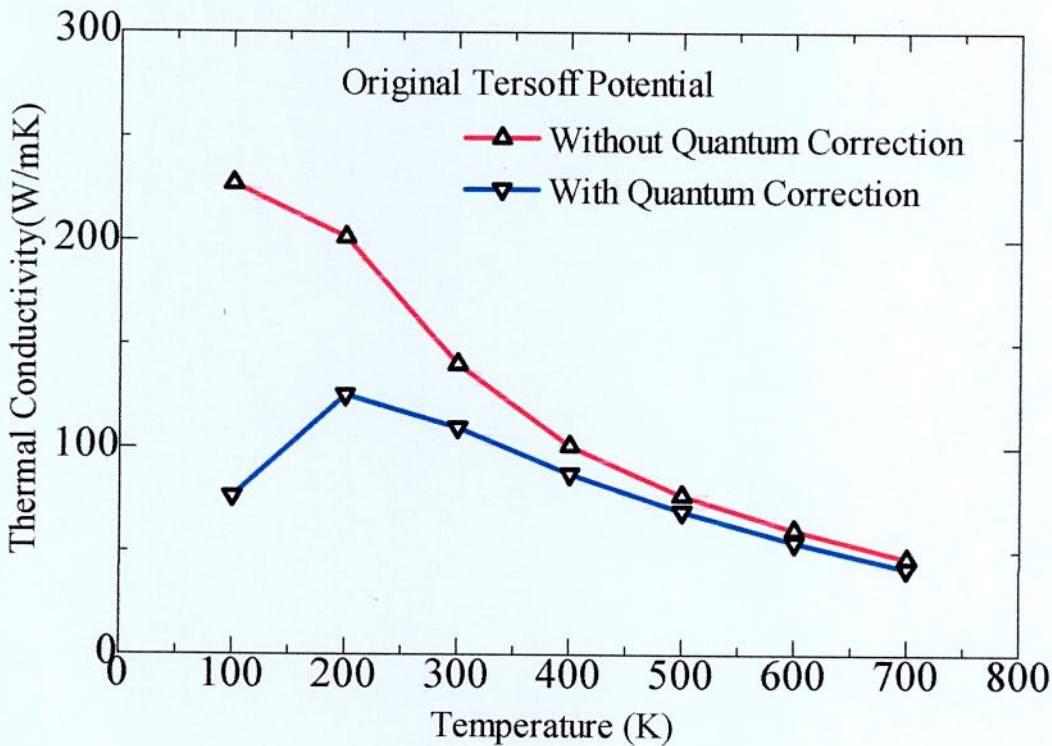
Figure 4.11: Temperature dependent thermal conductivity of 2D-SiC using original tersoff potential with and without quantum correction.
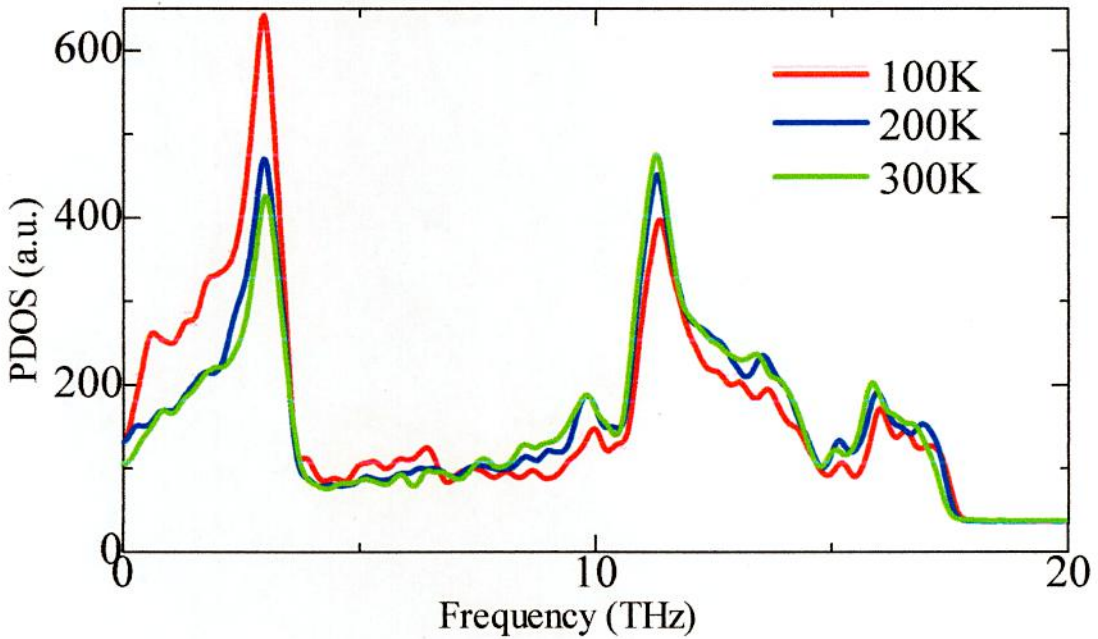
Figure 4.12: Temperature dependent acoustic phonon density of states of a 30 nm 2D-SiC sheet using velocity auto-correlation of atoms from 100 K to 300 K temperature.

occurred due to the increasing influence of LA and TA mode phonons with influence reduction of ZA mode phonons [60, 61]. Therefore, up to 207 K an increasing trend of the thermal conductivity may be occurred due to the increase of second and third peaks of PDOS results. On the other hand, a decrease of the first peak of the PDOS curve may be responsible for a lower value of thermal conductivity up to 207 K temperature when quantum corrections are applied.

4.3 Mechanical Behavior

Here the mechanical properties such as tensile strength and elastic modulus of both pristine and defected 2D-SiC sheets at different temperature and vacancy defect concentration are explored using molecular dynamics simulation. To ensure infinite 2D-SiC sheet, periodic boundary conditions are applied in both X and Y directions to remove the finite size effects. The stepwise straining method is used in the MD simulation to deform the nanosheet.

4.3.1 Effect of Temperature

2D-SiC is prospective to be used in several different applications for which the environmental conditions may vary considerably. In this section, the effect of different temperature varying from 300 K to 700 K on the mechanical properties of pristine 2D-SiC sheet is explored. The sheet length is considered as 30 nm in the X direction while width is fixed at 10 nm in the Y direction. A constant tensile engineering strain rate of 10^9 s^{-1} is chosen to deform the length at every time step of 1 fs. Fig. 4.13 shows the temperature dependent strain-stress behavior of pristine 2D-SiC sheet. The result shows a decrease of tensile strength with increase in temperature. From room temperature to higher temperature the fracture strain at which the sheet shows a failure is also decreased.
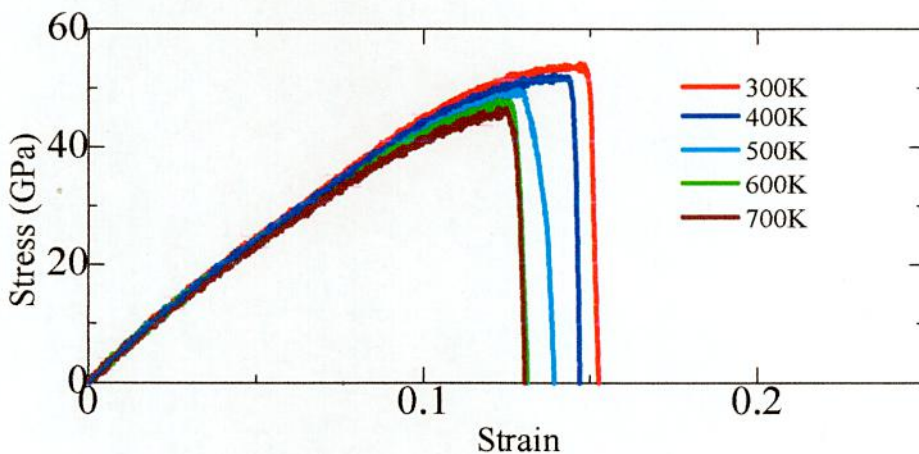
Figure 4.13: Strain-Stress behavior of pristine 2D-SiC from 300 K to 700 K temperature.

At 300 K temperature, the 2D-SiC sheet shows fracture strength of 53.625±7 GPa with a failure strain of 0.153, whereas at 700K the fracture strength is reduced to 45.9±7 GPa with fracture strain of 0.13. Increase of temperature from 300 K to 700 K, the fracture stress decreases 14.4% that of 53.625 GPa, whereas the fracture strain decreases 15.33% from the strain level of 0.153. At room temperature, the atomic vibration of 2D-SiC is not so obvious. However, with the increase of temperature the intensity of thermal vibration is so pronounced that the bond strength of the sheet shrinks considerably which affect the tensile strength of the 2D-SiC sheet.

In addition, at the primary deformation stage (up to about 0.05 strains), the stress increases linearly with strain. When the strain is increased to higher value, the strain–stress curve shows a nonlinear behavior. To explore the elastic modulus of 2D-SiC at different temperature condition the strain-stress relationship is fitted with the linear curve up to a very low strain level of < 0.05. Up to, this strain level the strain-stress curve shows elastic behavior. However, for larger strain level up to fracture strain the strain-stress curve shows plastic behavior. For temperature dependent elastic modulus characterization, the 2D-SiC shows a reduction of elastic modulus with room temperature to 700 K temperature.
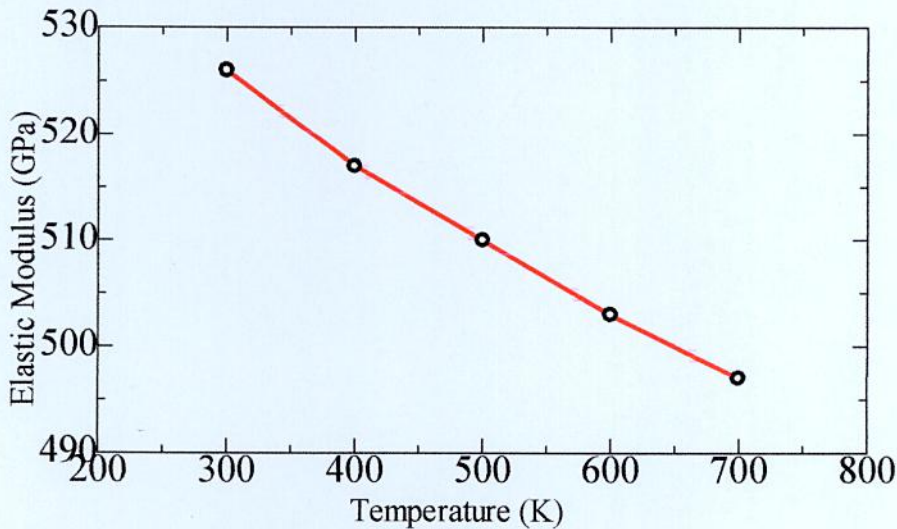
Figure 4.14: Elastic Modulus of pristine 2D-SiC from 300 K to 700 K temperature.

Fig. 4.14 shows a linear trend of reduction of temperature dependent elastic modulus behavior of 2D-SiC sheet. At room temperature, the elastic modulus is 526±10 GPa, which is reduced to 497±10 GPa at 700K temperature. Thus, all of the mechanical properties including the fracture strength, fracture strain and elastic modulus decrease significantly with the increase of temperature from 300 K to 700 K with an approximate reduction of 14.4% in the fracture strength, 15.3% in the fracture strain and 5.51% reduction in the elastic modulus. These results validate the choice of classical Vashishta potential and confirms the validity of this MD simulation for hexagonal 2D-SiC systems.

4.3.2 Effect of Defects

In realistic 2D-SiC material, several structural defects are permanently introduced as they are produced via mechanical exfoliation, chemical vapor deposition (CVD), or chemical reduction. Among these defects, vacancy defect is the most conquerable which changes the materials physical properties significantly. It was found that mechanical properties of 2D-SiC are considerably influenced by these defects. The nonexistence of atoms from the lattice of 2D-SiC is usually termed as vacancy defects, which can be further sub categorized as point-vacancy, bi-vacancy, and mixed-vacancy etc. centered on the number of atoms absent from the lattice. The absence of a single atom from the 2D-SiC sheet yields a point-vacancy defect, which left the 2D-SiC lattice with three under coordinated edge atoms, each of them possesses a single dangling bond; Removal of the highlighted atom in Fig. 4.15 (a), forming point-vacancy with metastable configuration. Moreover, the bi-vacancy defect can be created by the removal of two atoms from the pristine 2D-SiC as demonstrated in Fig. 4.15 (b). From Fig. 4.15 (a) (point-vacancy) and Fig. 4.15 (b) (bi-vacancy), it can be pointed out that after the restoration, under coordinated carbon/silicon atoms can be imagined only in point vacancy based structure, whereas for bi-vacancy based sheet there is no under coordinated carbon/silicon atoms. Thus, it can be said that point vacancy based sheet are less stable than bi-vacancy as there occurs metastable configuration due to the under coordinated atoms. Again the structure with mixed vacancy defect can be created when both the point vacancy and bi-vacancy defect occurs in the structure. Fig. 4.15 (c) shows the 2D-SiC sheet with mixed vacancy defects.
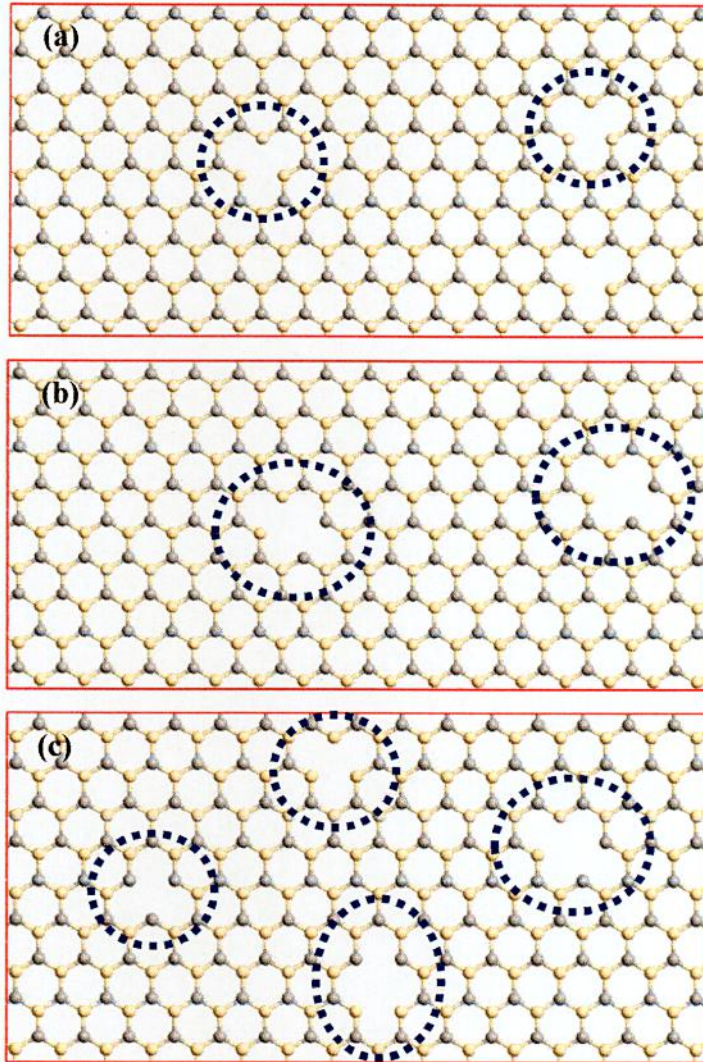
Figure 4.15: 2D-SiC sheet with a) point vacancy b) bi-vacancy c) mixed vacancy.

In this work, MD simulation is performed to explore the fracture behavior of 2D-SiC sheet with randomly distributed vacancy defects (bi-vacancy, point vacancy and mixed vacancy) with concentration of 0.1% to 1%. Fig. 4.16 (a-c) shows the fracture stress behavior of 2D-SiC at room temperature condition. In the results, it has been shown that the tensile strength decreases considerably with increasing defect concentration. For 0.1% bi-vacancy, the fracture strength reduced to 46.07 GPa from 53.625 GPa of pristine 2D-SiC. Furthermore, for 1% bi-vacancy, the fracture strength is reduced to 20.826 GPa, which is a 38.83% reduction from the pristine case.
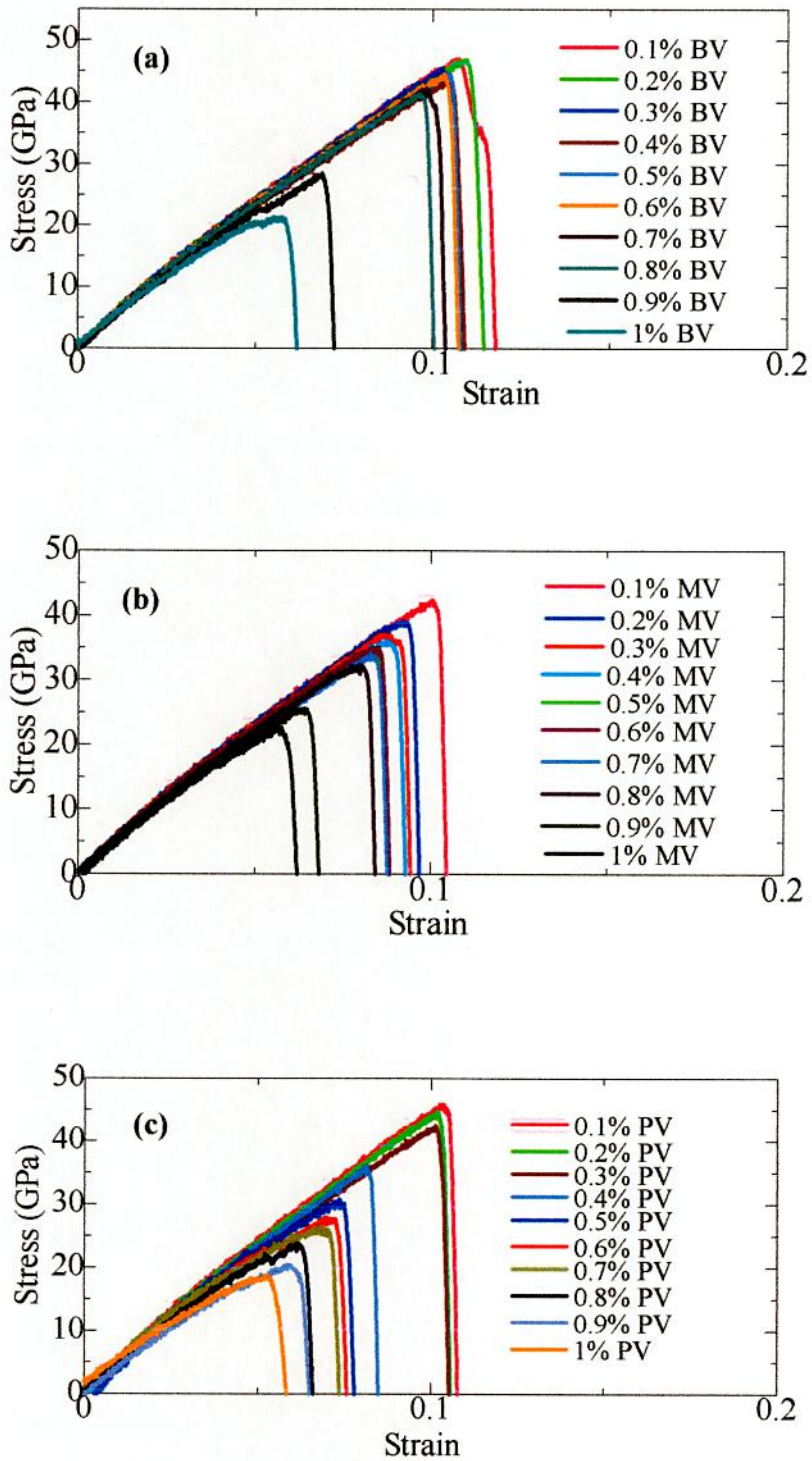
Figure 4.16: Strain-Stress behavior of 2D-SiC with.1% to 1% concentration of a) bi-vacancy b) mixed vacancy c) point vacancy.

Moreover, for mixed vacancy, the 2D-SiC shows a tensile strength of 42.04 GPa and 21.07 GPa, respectively for .1% and 1% vacancy concentration, whereas for point vacancy it is 44.87 GPa and 18.04 Gpa. From the results, it is found that for 1% vacancy, the tensile strength is reduced about 60.7% for mixed vacancy and 66.35% for point vacancy from that of pristine case.

Moreover, from the output of Fig. 4.17 it is observed that up to 0.4% vacancy concentration there is a small variation in the tensile strength behavior of different vacancy defected 2D-SiC. However, when the defect concentration has increased more than 0.5%, the fracture strength and fracture strain of 2D-SiC are significantly differ with each other and an inclusive lessening trend is perceived for both of fracture strength and strain at failure. Here, the point vacancy defect shows the tremendous effect on the fracture behavior due to the symmetry breakdown of the SiC sheet at larger scale compared to mixed and bi-vacancy defects. Here, the vacancy concentration based elastic modulus of defected 2D-SiC is also investigated, which is shown in Fig. 4.18. To investigate the elastic modulus, the linear portion of the strain - stress curve up to 0.03 strain levels is considered. The results show that, in all cases by growing the defect concentration, elastic modulus shrinkages regularly. Lessening of elastic modulus is more substantial in the case of point vacancy and mixed vacancy. In these cases, elastic modulus declines by around 17.5% and 15.4% for 1% vacancy concentration which is almost 1.5 intervals greater than the same concentration of bi-vacancy defects.
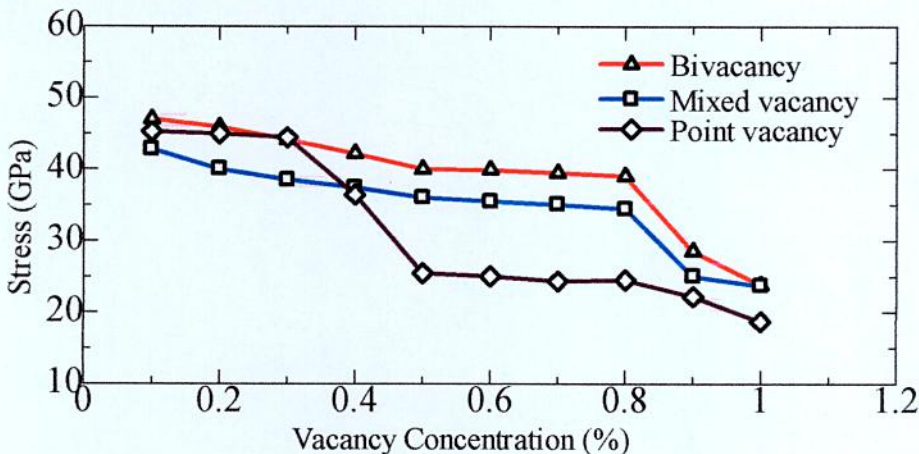
Figure 4.17: Vacancy concentration dependent Strain-Stress behavior of 2D-SiC.
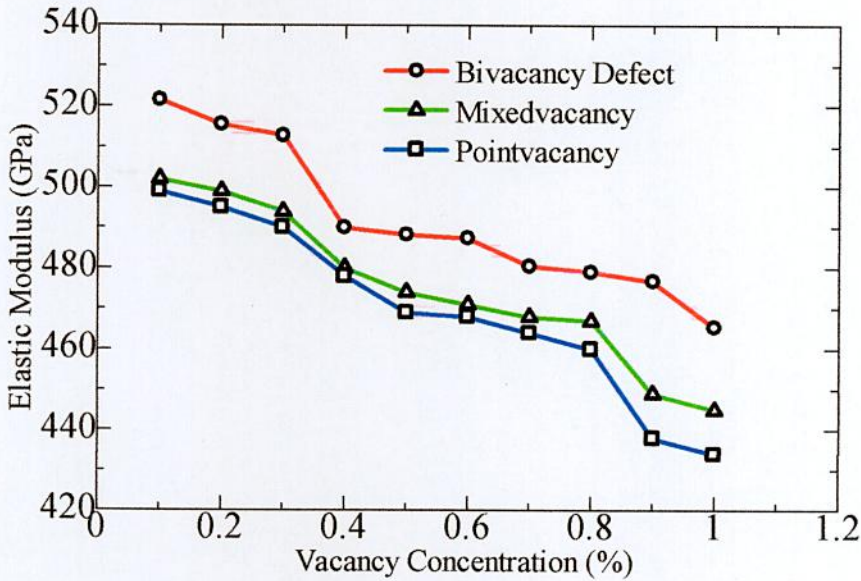
Figure 4.18: Vacancy concentration dependent Elastic Modulus of 2D-SiC.

4.3.3 Effect of Defects and Temperature

The fracture strength and elastic modulus of 2D-SiC from room temperature to 700 K temperature with 0.5% vacancy defect are also explored here. The combined effect of temperature and vacancy significantly reduces the fracture strength and elastic modulus of the 2D-SiC sheet. At 700 K temperature with 0.5% bi-vacancy, the fracture strength and elastic modulus are reduced to 31.06 GPa and 432 GPa, respectively from 53.625 GPa and 526 GPa of the pristine sheet of 300 K temperature. In Fig 4.20, acquired stress–strain response of 2D-SiC with 0.5% concentration of point vacancy, bi-vacancy and mixed-vacancy with temperature variation from 300 K to 700 K are illustrated. From the results, it has been seen that, the fracture stress decreases more significantly for point vacancy than other types of vacancy defects. On the other hand, it is observed that effect of mixed vacancy and bi-vacancy defects on the tensile strength and failure strain of 2D-SiC are considerably closer to each other. In addition, for 700 K temperature with 0.5% concentration of point vacancy defect the elastic modulus decreases around 18.9% than pristine case which is shown in Fig. 4.21. For bi-vacancy defects, it is found
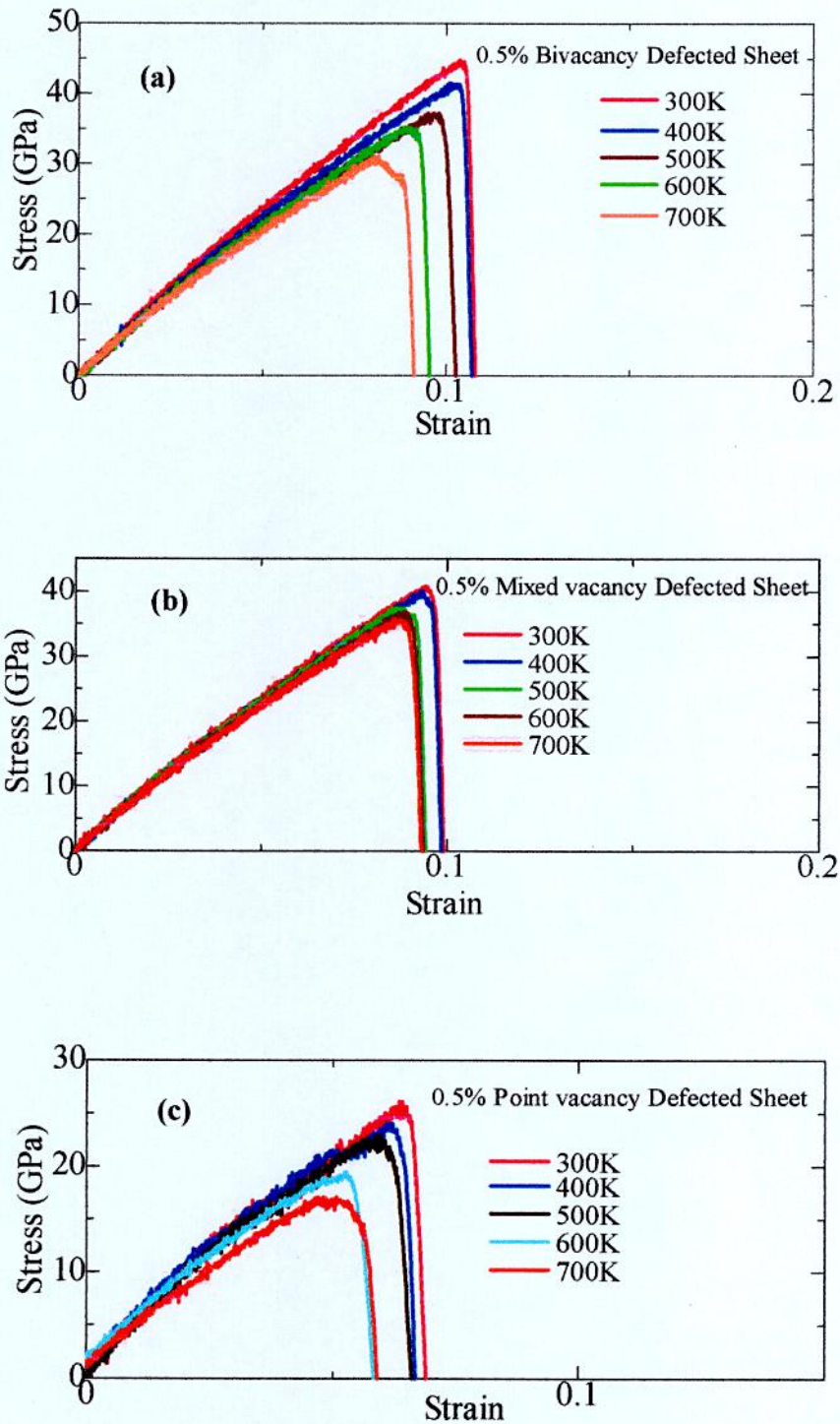
Figure 4.19: Temperature dependent Strain-Stress behaviors of a) 0.5% bi-vacancy defected 2D-SiC b) 0.5% mixed vacancy defected 2D-SiC c) 0.5%-point vacancy defected 2D-SiC.

that up to low vacancy concentrations (0.5%) elastic modulus is very close to that of the mixed vacancy result. Furthermore, with the increase of defect concentration, the elastic modulus gets closer to that of the point vacancy defect result. In comparison with a recent structural molecular mechanic's study [103], the results of this work suggest considerable effects of the vacancy defects on the elastic properties of 2D-SiC system due to proper parameterization with Vashishta potential.
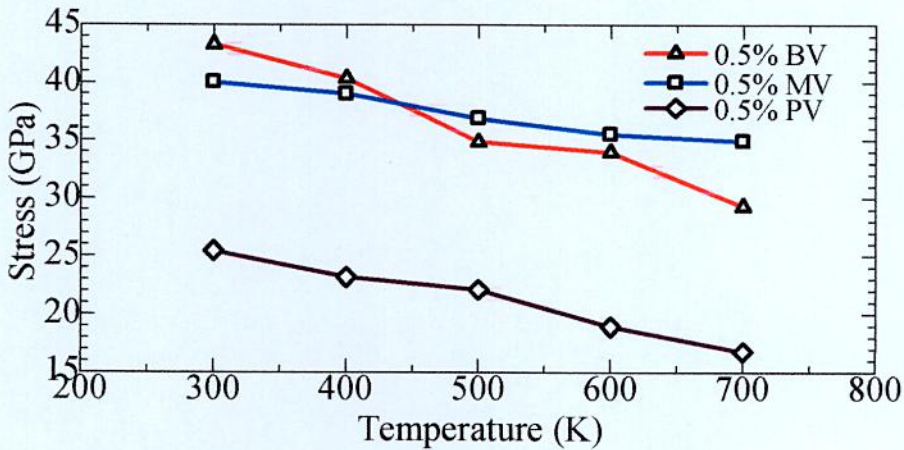
Figure 4.20: Temperature dependent Strain-Stress behavior of 0.5% vacancy defected 2D-SiC.
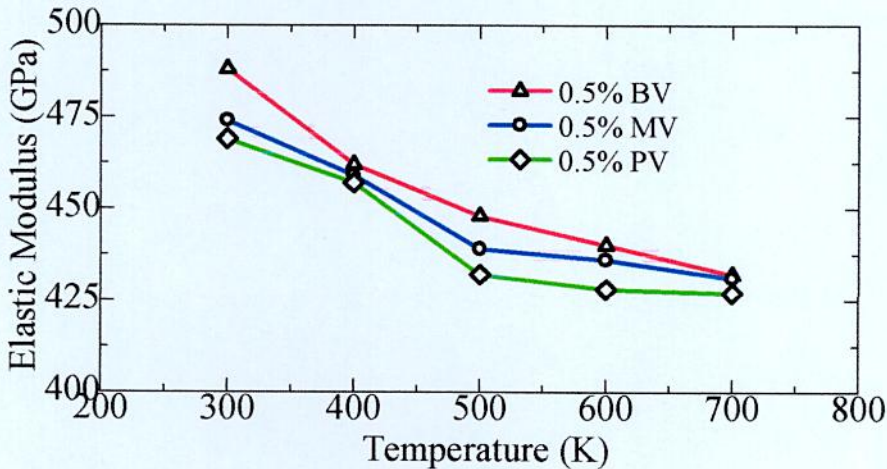
Figure 4.21: Temperature dependent Elastic Modulus of 0.5% Vacancy defected 2D-SiC.

4.3.4 Rupturing Process

To reveal how the pristine and defective 2D-SiC ruptures, the progression of the microstructure is explored using OVITO package. In Fig. 4.22, distortion development of defect free 2D-SiC is shown at numerous strain stages. It is observed that in the case of defect free 2D-SiC, sample prolongs consistently and remains unharmed up to the fracture strength point (Fig. 4.22). The fracture strength is a point at which the first de-bonding happens concerning two neighboring atoms. Soon after, the development of the initial void and extension of this defective area along the sample is perceived (Fig. 4.22). Here the preliminary voids are confined and the left behind part of the sample leftovers uncontaminated. The main characteristic of these initially formed voids is the formation of monoatomic chains of carbon and silicon atoms. It can be noted that the Vashishta potential suggests the deformation process of 2D-SiC to be purely brittle and only limited mono-atomic chains during failure process are formed [85, 86]. From Fig. 4.21 it is seen that, mono-atomic chains are formed along the zigzag direction and initial de-bonding are also occurred along the zigzag direction. By increasing the strain levels, the initiations of more voids
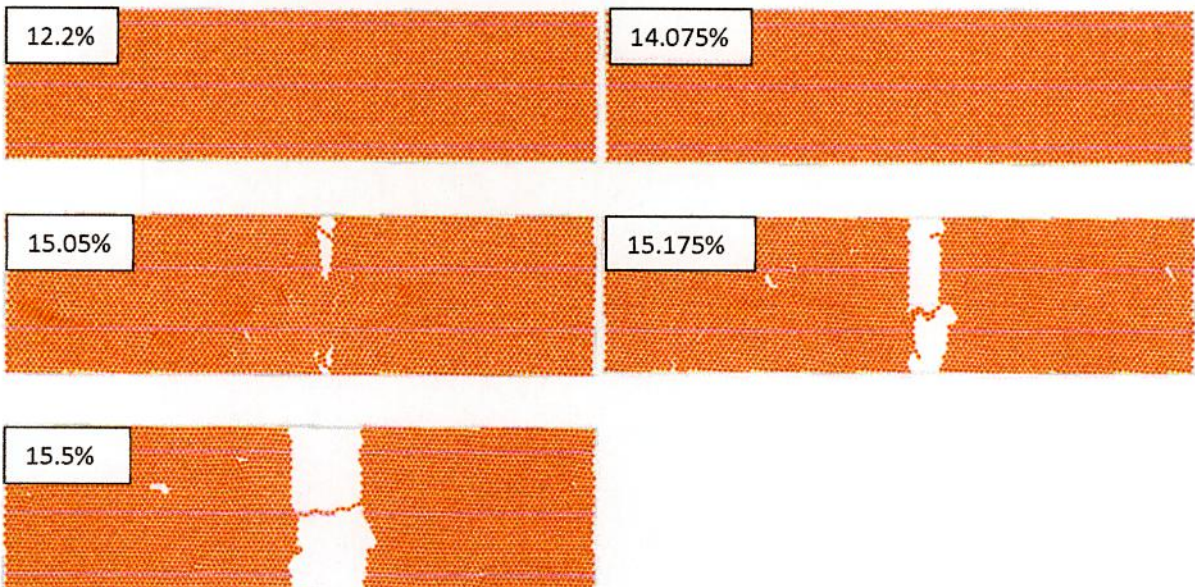
Figure 4.22: Rupturing process for pristine 2D-SiC.

are found. In addition, the elongations of mono-atomic chains that tend to keep the 2D-SiC sheet connected are also observed. The final rupture occurs when the last connecting mono-atomic chain fails (Fig. 4.22). As shown in Fig. 4.22, in the ruptured 2D-SiC sheets, edges are mainly along the zigzag direction. When the applied strain exceeds a critical value of $\varepsilon = 0.155$, one of these two most dangerous bonds is broken stochastically, leading to the destruction of the structure. As the strain further increases from $\varepsilon = 0.155$ to $\varepsilon = 0.156$, bonds exhibit successive rupture. These observations suggest that the proposed molecular dynamics scheme is considerably accurate for the evaluation of the mechanical response of 2D-SiC.

The defective 2D-SiC sheets show the similar trend of fracture behavior like pristine 2D-SiC. In the case of bi-vacancy defects, at strain levels lower than the tensile strength limit, the formation of ten-membered carbon-silicon rings are observed in the places where two bi-vacancy defects are connected together by only one C/Si bonds (Fig. 4.23). Unlike defect-free 2D-SiC sheet, in the case of bi- vacancy defect, damage of 2D-SiC is more localized and the rest of the 2D-SiC sheet remains almost undamaged. Similar types of rupturing process are also occurred for mixed vacancy and point vacancy defect. For point vacancy defect the process start at very smaller strain level than bi-vacancy and mixed vacancy defects due to the larger symmetry breakdown in different portions of the sheet.
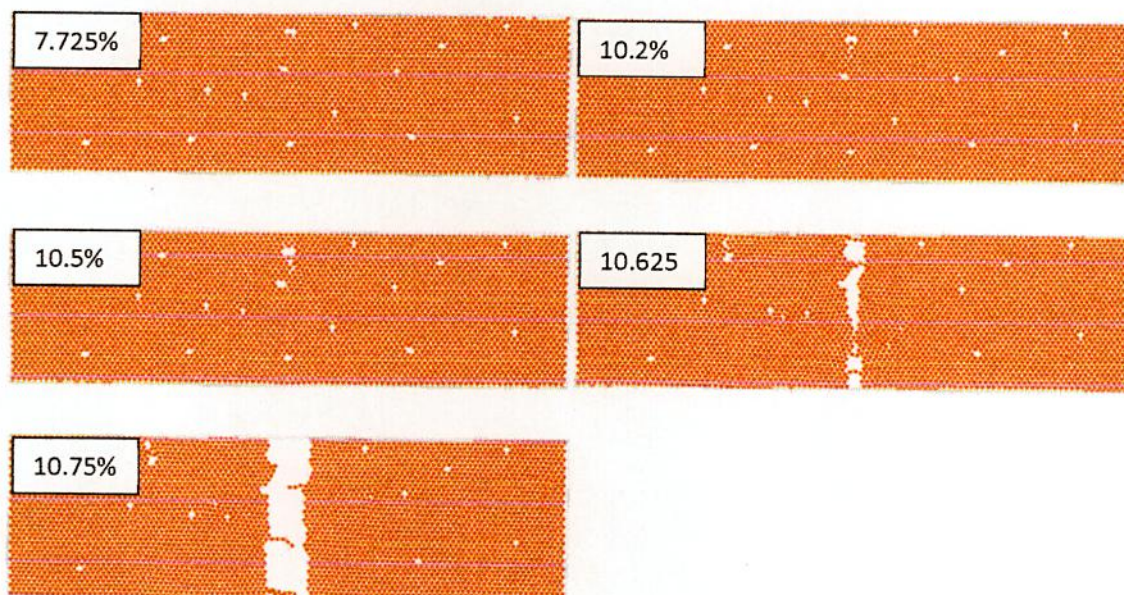
Figure 4.23: Rupturing process for bi-vacancy defected 2D-SiC.
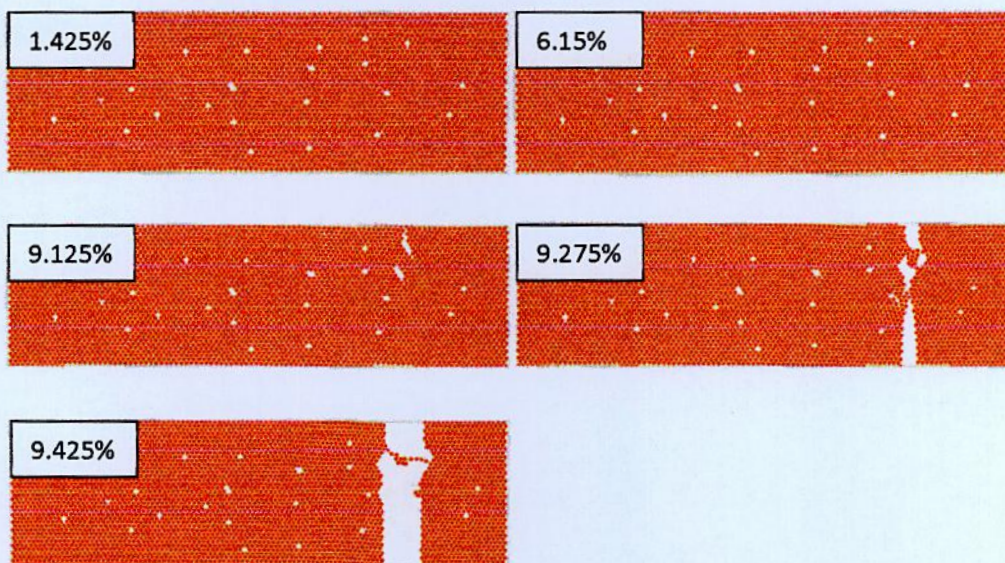
Figure 4.24: Rupturing process for mixed vacancy defected 2D-SiC.
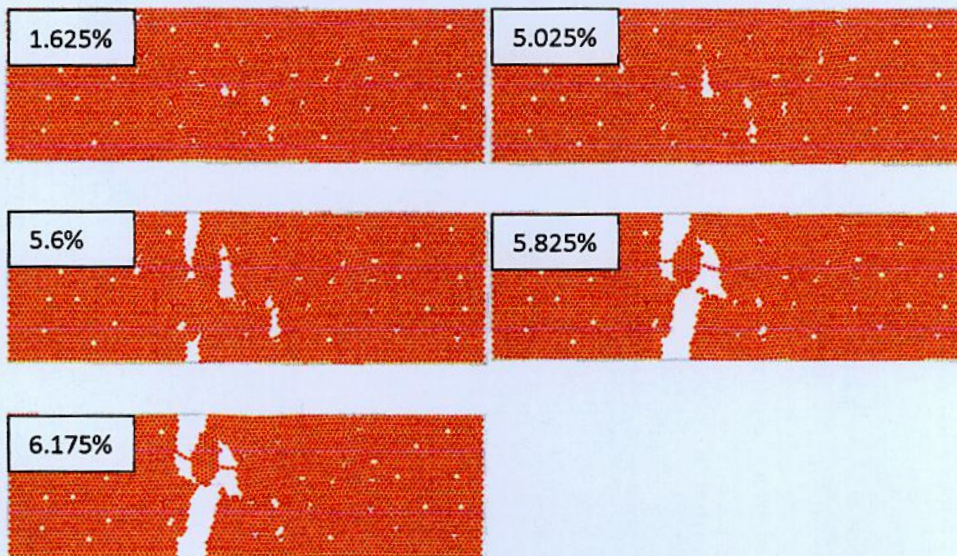
Figure 4.25: Rupturing process for point vacancy defected 2D-SiC.

CHAPTER V

Conclusion and Future Outlook

5. 1 Conclusion

This dissertation focused on the effects of length and temperature on the thermal conductivity of the 2D-SiC sheet using non-equilibrium molecular dynamics simulation. The original as well as optimized tersoff potentials have employed to clarify their impact on the thermal conductivity of 2D-SiC. In addition, the effects of different temperature and vacancy defects on the mechanical behavior of 2D-SiC have been explored using virial stress dependent molecular dynamics simulation.

The outcome of non-equilibrium molecular dynamics simulation gives exceptional results of thermal conductivity of 2D-SiC at different length and temperature. It is perceived that the classical potential has the significant effects on the thermal conductivity of 2D-SiC. The optimized tersoff potential gives a better estimation of thermal conductivity than the original potential due to proper parameterization with analytical model. The phonon density of states shows a strengthening behavior of the acoustic phonon peaks when the length is increased. Moreover, due to the variation of Debye temperature, acoustic modes group velocities and strong polarization effects of binary 2D-SiC, a thermal conductivity of 271.03 W/mK is found at 600 nm length for optimized tersoff potential which is much greater than silicene but lower than graphene. Above room temperature, an anomalous decreasing trend of thermal conductivity is attained for both optimized and original tersoff potential due to the influence of Umklapp limited phonon scattering and reduction of FA mode phonons. Besides, a shrinking trend of frequency spectrum is noticed from the temperature dependence PDOS curve which quantifies the reduction of the thermal conductivity at high temperature. On the other hand, due to the consideration of ground state phonon modes in specific heat capacity, an increasing trend of thermal conductivity is achieved up to Debye temperature when quantum corrections are applied.

Moreover, due to the thermal variation effects, a decreasing behavior of the mechanical properties of 2D-SiC such as tensile strength and elastic modulus is perceived when temperature is increased from 300 K to 700 K. It was observed that at temperature 300 K to 700K, the

fracture stress and fracture strain decreases as 14.4% and 15.33%, respectively from the pristine case. In addition, due to symmetry breakdown and bond breaking phenomena produced by the vacancy defects, linear reduction trend of the mechanical properties is found. It has also been explored that point vacancy creates most traitorous effect on the fracture behavior than bi-vacancy and mixed vacancy defect due to the greater symmetry breakdown of same concentrations. In the case of point vacancy elastic modulus decreases by ~ 17.5% for 1% vacancy concentration which is almost 1.5 times higher than the same concentration of bi-vacancy defects. Besides, the progression of microstructure rupturing for both the pristine and defective 2D-SiC is also discovered here at different strain levels. It is observed that in both cases, specimen extends uniformly and remains undamaged up to the tensile strength point. These results provide a new insight for the effective thermal and mechanical design of SiC based nanodevices and nanoelectromechanical systems.

5.2 Future Work

The molecular dynamics simulation technique described in this dissertation has proven to be an intriguing tool to describe the thermal, mechanical and phonon properties of 2D-SiC. At the same time, there have been several important issues in the field that remain to be addressed. The thermal conductivity of 2D-SiC considering various types of defects can be calculated. The thermal conductivity of the layered structure of SiC and different hetero-structures based on SiC materials can be investigated. Furthermore, the elastic behavior of different binary 2D materials, hetero-structures, layered materials can be explored by considering the effects of doping, vacancy and other types of variations.

References

[1]   O. Semenov, A. Vassighi, and M. Sachdev, "Impact of self-heating effect on long-term reliability and performance degradation in CMOS circuits," *IEEE Transactions on Device and Materials Reliability,* vol. 6, no. 1, pp. 17-27, 2006.

[2]   E. Pop, "Energy dissipation and transport in nanoscale devices," *Nano Research,* vol. 3, no. 3, pp. 147-169, 2010/03/01 2010.

[3]   L. N. Denis and A. B. Alexander, "Two-dimensional phonon transport in graphene," *Journal of Physics: Condensed Matter,* vol. 24, no. 23, p. 233203, 2012.

[4]   R. Stevenson, "Changing the channel," IEEE Spectrum ,vol. 50, no. 7, pp. 34-39, 2013.

[5]   H. Zhao and N. R. Aluru, "Temperature and strain-rate dependent fracture strength of graphene," *Journal of Applied Physics,* vol. 108, no. 6, p. 064321, 2010.

[6]   M. Xu, T. Liang, M. Shi, and H. J. Chen, "Graphene-like two-dimensional materials," *Chem. Rev.,* vol. 113, no. 5, pp. 3766-3798, 2013.

[7]   S. Z. Butler *et al.*, "Progress, challenges, and opportunities in two-dimensional materials beyond graphene," *ACS Nano,* vol. 7, no. 4, pp. 2898-2926, 2013.

[8]   Q. H. Wang, K. Kalantar-Zadeh, A. Kis, J. N. Coleman, and M. S. Strano, "Electronics and optoelectronics of two-dimensional transition metal dichalcogenides," *Nat. Nanotechnol.,* vol. 7, no. 11, p. 699, 2012.

[9]   M. Chhowalla, H. S. Shin, G. Eda, L. Li, K. P. Loh, and H. J. Zhang, "The chemistry of two-dimensional layered transition metal dichalcogenide nanosheets," *Nat. Chem.,* vol. 5, no. 4, p. 263, 2013.

[10]   S. Cahangirov, M. Topsakal, E. Aktürk, H. Şahin, and S. Ciraci, "Two-and one-dimensional honeycomb structures of silicon and germanium," *Phys Rev Lett.,* vol. 102, no. 23, p. 236804, 2009.

[11]   A. Fleurence, R. Friedlein, T. Ozaki, H. Kawai, Y. Wang, and Y. J. Yamada-Takamura, "Experimental evidence for epitaxial silicene on diboride thin films," *Phys Rev Lett.,* vol. 108, no. 24, p. 245501, 2012.

[12]   P. J. Vogt, "P. Vogt, P. De Padova, C. Quaresima, J. Avila, E. Frantzeskakis, MC Asensio, A. Resta, B. Ealet, and G. Le Lay, *Phys. Rev. Lett.*, vol. 108, p. 155501, 2012.

[13]   B. Wang *et al.*, "Stable planar single-layer hexagonal silicene under tensile strain and its anomalous Poisson's ratio," *Appl Phys Lett.,* vol. 104, no. 8, p. 081902, 2014.

[14]   K. S. Novoselov *et al.*, "Electric field effect in atomically thin carbon films," *Science,* vol. 306, no. 5696, pp. 666-669, 2004.

[15]   K. S. Novoselov *et al.*, "Two-dimensional gas of massless Dirac fermions in graphene," *Nature,* vol. 438, no. 7065, p. 197, 2005.

[16]   B. Lalmi *et al.*, "Epitaxial growth of a silicene sheet," *Appl. Phys. Lett.,* vol. 97, no. 22, p. 223109, 2010.

[17]   X. Lin *et al.*, "Ab initio study of electronic and optical behavior of two-dimensional silicon carbide," *J. Mater. Chem. C,* vol. 1, no. 11, pp. 2131-2135, 2013.

[18]   S. Balendhran, S. Walia, H. Nili, S. Sriram, and M. J. Bhaskaran, "Elemental analogues of graphene: silicene, germanene, stanene, and phosphorene," *Small,* vol. 11, no. 6, pp. 640-652, 2015.

[19]   H. Hsueh, G. Guo, and S. G. Louie, "Excitonic effects in the optical properties of a SiC sheet and nanotubes," *Phys. Rev. B: Condens. Matter Mater. Phys.,* vol. 84, no. 8, p. 085404, 2011.

65

[20] E. Fortin, S. Fafard, and A. Mysyrowicz, "Exciton transport in Cu_2O: Evidence for excitonic superfluidity?," *Phys. Rev. Lett.*, vol. 70, no. 25, p. 3951, 1993.
[21] P. Lou and J. Lee, "Spin controlling in narrow zigzag silicon carbon nanoribbons by carrier doping," *J. Phys. Chem. C*, vol. 114, no. 24, pp. 10947-10951, 2010.
[22] T.Y. Lü, X. X. Liao, H. Q. Wang, and M. C. Zheng, "Tuning the indirect–direct band gap transition of SiC, GeC and SnC monolayer in a graphene-like honeycomb structure by strain engineering: a quasiparticle GW study," *J. Mater. Chem.*, vol. 22, no. 19, pp. 10062-10068, 2012.
[23] L. Sun *et al.*, "Electronic structures of SiC nanoribbons," *J. Chem. Phys.*, vol. 129, no. 17, p. 174114, 2008.
[24] K. J. Wonchutigul, "Properties of Silicon carbide, edited by GL Harris," vol. 13, p. 136, 1995.
[25] Y. Yang *et al.*, "Monocrystalline silicon carbide nanoelectromechanical systems," *Applied Physics Lett.*, vol. 78, no. 2, pp. 162-164, 2001.
[26] T. Susi *et al.*, "Computational insights and the observation of SiC nanograin assembly: towards 2D silicon carbide," *Scientific Reports*, vol. 7, no. 1, p. 4399, 2017.
[27] Z. Shi, Z. Zhang, A. Kutana, and B. Yakobson, "Predicting two-dimensional silicon carbide monolayers," *ACS Nano*, vol. 9, no. 10, pp. 9802-9809, 2015.
[28] Z. Xu, Y. Li, and Z. Liu, "First-principles calculations of structural, electronic, and thermodynamic properties of monolayer $Si_{1-x}Ge_xC$ sheet," *RSC Adv.*, vol. 6, no. 115, pp. 113903-113910, 2016.
[29] S. Lin *et al.*, "Quasi-two-dimensional sic and sic2: Interaction of silicon and carbon at atomic thin lattice plane," *J. Phys. Chem. C*, vol. 119, no. 34, pp. 19772-19779, 2015.
[30] T. Miao, S. Yeom, P. Wang, B. Standley, and M. Bockrath, "Graphene nanoelectromechanical systems as stochastic-frequency oscillators," *Nano Letters*, vol. 14, no. 6, pp. 2982-2987, 2014.
[31] X. Xu *et al.*, "Length-dependent thermal conductivity in suspended single-layer graphene," *Nature Communications*, vol. 5, p. 3689, 2014.
[32] D. L. Nika and A. A. Balandin, "Two-dimensional phonon transport in graphene," *Journal of Physics: Condensed Matter*, vol. 24, no. 23, p. 233203, 2012.
[33] H. Zhao, K. Min, and N. J. Aluru, "Size and chirality dependent elastic properties of graphene nanoribbons under uniaxial tension," *Nano Letters*, vol. 9, no. 8, pp. 3012-3015, 2009.
[34] A. Taloni, M. Vodret, G. Constantini, and S. J. Zapperi, "Size effects on the fracture of microscale and nanoscale materials," *Nature reviews| Materials*, vol. 3, pp. 211-224, 2018.
[35] X. Xu, J. Chen, and B. Li, "Phonon thermal conduction in novel 2D materials," *Journal of Physics: Condensed Matter*, vol. 28, no. 48, p. 483001, 2016.
[36] E. Pop, S. Sinha, and K. Goodson, "Heat generation and transport in nanometer-scale transistors," *Proceedings of the IEEE*, vol. 94, no. 8, pp. 1587-1601, 2006.
[37] D. J. Miller, "Device requirements for optical interconnects to silicon chips," *Proceedings of the IEEE*, vol. 97, no. 7, pp. 1166-1185, 2009.
[38] A. Sarua *et al.*, "Thermal boundary resistance between GaN and substrate in AlGaN/GaN electronic devices," *IEEE Transactions on Electron Devices*, vol. 54, no. 12, pp. 3152-3158, 2007.

[39] E. Pop, V. Varshney, and A. Roy, "Thermal properties of graphene: Fundamentals and applications," *MRS Bulletin*, vol. 37, no. 12, pp. 1273-1281, 2012.

[40] Y. Lin and J. Connell, "Advances in 2D boron nitride nanostructures: nanosheets, nanoribbons, nanomeshes, and hybrids with graphene," *Nanoscale*, vol. 4, no. 22, pp. 6908-6939, 2012.

[41] X. Wei *et al.*, "Phonon thermal conductivity of monolayer MoS2: A comparison with single layer graphene," *Applied Physics Letters*, vol. 105, no. 10, p. 103902, 2014.

[42] A. Cao, "Molecular dynamics simulation study on heat transport in monolayer graphene sheet with various geometries," *J. Appl. Phys.*, vol. 111, no. 8, p. 083528, 2012.

[43] A. A. Balandin *et al.*, "Superior thermal conductivity of single-layer graphene," *Nano Lett.*, vol. 8, no. 3, pp. 902-907, 2008.

[44] D. A. Borca-Tasciuc, WL Liu, G. Chen, H.W. Ren, C.H. Lin, SS Pei,"Thermal conductivity of lnAs/AlSb superlattices," *Microscale Termophys. Eng.*, vol. 5, no. 3, pp. 225-231, 2001.

[45] A. Balandin and K. Wang, "Significant decrease of the lattice thermal conductivity due to phonon confinement in a free-standing semiconductor quantum well," *Phys. Rev. B.*, vol. 58, no. 3, p. 1544, 1998.

[46] G. Basile, C. Bernardin, and S. Olla, "Momentum conserving model with anomalous thermal conductivity in low dimensional systems," *Phys. Rev. Lett.*, vol. 96, no. 20, p. 204303, 2006.

[47] D. Akinwande *et al.*, "A review on mechanics and mechanical properties of 2D materials—Graphene and beyond," *Extreme Mechanics Letters*, vol. 13, pp. 42-77, 2017.

[48] J. Xiao, J. Staniszewski, J. Gillespie Jr, and E. A, "Tensile behaviors of graphene sheets and carbon nanotubes with multiple Stone–Wales defects," *Mater Sci. Eng. A*, vol. 527, no. 3, pp. 715-723, 2010.

[49] G.D. Lee, C. Wang, E. Yoon, N.M. Hwang, D.Y. Kim, and K. Ho, "Diffusion, coalescence, and reconstruction of vacancy defects in graphene layers," *Phys Rev Lett*, vol. 95, no. 20, p. 205501, 2005.

[50] A. Zandiatashbar *et al.*, "Effect of defects on the intrinsic strength and stiffness of graphene," *Nat Commun*, vol. 5, p. 3186, 2014.

[51] X. Qi-lin, L. Zhen-huan, and T. Xiao-geng, "The defect-induced fracture behaviors of hexagonal boron-nitride monolayer nanosheets under uniaxial tension," *J. Phys. D: Appl. Phys.*, vol. 48, no. 37, p. 375502, 2015.

[52] J. Zhang, T. Ragab, and C. Basaran, "The effects of vacancy defect on the fracture behaviors of zigzag graphene nanoribbons," *International Journal of Damage Mechanics*, vol. 26, no. 4, pp. 608-630, 2017.

[53] M. An, Q. Deng, Y. Li, H. Song, M. Su, "The effect of defects on the fracture behavior of trilayer graphene," *Superlattices and Microstructures*, vol. 123, pp. 172-182, 2018.

[54] S.D. Guo, J. Dong, and J. Liu, "Nonmonotonic strain dependence of lattice thermal conductivity in monolayer SiC: a first-principles study," *Phys. Chem. Chem. Phys.*, vol. 20, no. 34, pp. 22038-22046, 2018.

[55] A. A. Balandin, "Thermal properties of graphene and nanostructured carbon materials," *Nature Materials.*, vol. 10, no. 8, p. 569, 2011.

[56] B. Peng, H. Zhang, H. Shao, Y. Xu, X. Zhang, and H. Zhu, "Low lattice thermal conductivity of stanene," *Sci. Rep.*, vol. 6, p. 20225, 2016.

[57] D. Nika, E. Pokatilov, A. Askerov, and A. Balandin, "Phonon thermal conduction in graphene: Role of Umklapp and edge roughness scattering," *Phys. Rev. B*, vol. 79, no. 15, p. 155413, 2009.

[58] A. Alofi and G. Srivastava, "Thermal conductivity of graphene and graphite," *Phys. Rev. B*, vol. 87, no. 11, p. 115421, 2013.

[59] G. Qin, Z. Qin, H. Wang, and M. Hu, "Anomalously temperature-dependent thermal conductivity of monolayer GaN with large deviations from the traditional 1/T law," *Phys. Rev. B*, vol. 95, no. 19, p. 195416, 2017.

[60] Z. Qin, G. Qin, X. Zuo, Z. Xiong, and M. Hu, "Orbitally driven low thermal conductivity of monolayer gallium nitride (GaN) with planar honeycomb structure: a comparative study," *Nanoscale*, vol. 9, no. 12, pp. 4295-4309, 2017.

[61] H. Wang, G. Qin, G. Li, Q. Wang, and M. Hu, "Low thermal conductivity of monolayer ZnO and its anomalous temperature dependence," *Phys. Chem. Chem. Phys.*, vol. 19, no. 20, pp. 12882-12889, 2017.

[62] H. Zaoui, P. L. Palla, F. Cleri, and E. Lampin, "Length dependence of thermal conductivity by approach-to-equilibrium molecular dynamics," *Physical Review B*, vol. 94, no. 5, p. 054304, 2016.

[63] D. L. Nika, A. S. Askerov, and A. A. Balandin, "Anomalous size dependence of the thermal conductivity of graphene ribbons," *Nano Lett.*, vol. 12, no. 6, pp. 3238-3244, 2012.

[64] N. Mingo and D. Broido, "Length dependence of carbon nanotube thermal conductivity and the "problem of long waves", *Nano Lett.*, vol. 5, no. 7, pp. 1221-1225, 2005.

[65] R. Saito, M. Masashi, and M. Dresselhaus, "Ballistic and Diffusive Thermal Conductivity of Graphene," *Physical Review Applied*, vol. 9, no. 2, p. 024017, 2018.

[66] M. Jiang, J. Zheng, H. Xiao, Z. Liu, and X. Zu, "A comparative study of the mechanical and thermal properties of defective ZrC, TiC and SiC," *Scientific Reports*, vol. 7, no. 1, p. 9344, 2017.

[67] M. A. Makeev, D. Srivastava, and M. Menon, "Silicon carbide nanowires under external loads: An atomistic simulation study," *Phys Rev B*, vol. 74, no. 16, p. 165303, 2006.

[68] B. Baumeier, P. Krüger, and J. Pollmann, "Structural, elastic, and electronic properties of SiC, BN, and BeO nanotubes," *Physical Review B*, vol. 76, no. 8, p. 085407, 2007.

[69] A. Setoodeh, M. Jahanshahi, and H. Attariani, "Atomistic simulations of the buckling behavior of perfect and defective silicon carbide nanotubes," *Computational Materials Science*, vol. 47, no. 2, pp. 388-397, 2009.

[70] S. Chabi, H. Chang, Y. Xia, and Y. Zhu, "From graphene to silicon carbide: ultrathin silicon carbide flakes," *Nanotechnology*, vol. 27, no. 7, p. 075602, 2016.

[71] D.T. Nguyen, M. Le, "Mechanical properties of various two-dimensional silicon carbide sheets: an atomistic study," *Superlattices and Microstructures*, vol. 98, pp. 102-115, 2016.

[72] M.Q. Le, D. Nguyen, and E. A, "Atomistic simulations of pristine and defective hexagonal BN and SiC sheets under uniaxial tension," *Materials Science and Engineering: A*, vol. 615, pp. 481-488, 2014.

[73] M.Q. Le, "Atomistic study on the tensile properties of hexagonal AlN, BN, GaN, InN and SiC sheets," *Journal of Computational and Theoretical Nanoscience*, vol. 11, no. 6, pp. 1458-1464, 2014.

[74]   W. J. Choyke, H. Matsunami, and G. Pensl, Silicon carbide: recent major advances. *Springer Science & Business Media*, 2013.

[75]   P. Zhou, and X. Zeng, "The search for the most stable structures of silicon–carbon monolayer compounds," *Nanoscale,* vol. 6, no. 20, pp. 11685-11691, 2014.

[76]   J. Schön and A. Ceramics, "Nanomaterials-What energy landscapes can tell us," *Processing and Application of Ceramics*, vol. 9, no. 3, pp. 157-168, 2015.

[77]   E. Bekaroglu, M. Topsakal, S. Cahangirov, and S. J. P. R. B. Ciraci, "First-principles study of defects and adatoms in silicon carbide honeycomb structures", vol. 81, no. 7, p. 075433, 2010.

[78]   H. Şahin *et al.*, "Monolayer honeycomb structures of group-IV elements and III-V binary compounds: First-principles calculations," vol. 80, no. 15, p. 155453, 2009.

[79]   X. Lin *et al.*, "Optical and electronic properties of two dimensional graphitic silicon carbide," 2012.

[80]   B. Alder and T. Wainwright, "Phase transition for a hard sphere system," *The Journal of Chemical Physics*, vol. 27, no. 5, pp. 1208-1209, 1957.

[81]   D. C. Rapaport and D. Rapaport, *The art of molecular dynamics simulation. Cambridge university press*, 2004.

[82]   H. J. Berendsen, J. Postma, W. F. van Gunsteren, A. Dinola, and J. Haak, "Molecular dynamics with coupling to an external bath," *The Journal of Chemical Physics*, vol. 81, no. 8, pp. 3684-3690, 1984.

[83]   P. H. Hünenberger, "Thermostat algorithms for molecular dynamics simulations," in *Advanced computer simulation: Springer*, 2005, pp. 105-149.

[84]   D. J. Evans and B. Holian, "The nose–hoover thermostat," *The Journal of Chemical Physics*, vol. 83, no. 8, pp. 4069-4074, 1985.

[85]   W. Hoover, "Canonical dynamics: equilibrium phase-space distributions," *Phys. Rev. A*, vol. 31, no. 3, p. 1695, 1985.

[86]   S. Nosé, "A unified formulation of the constant temperature molecular dynamics methods," *The Journal of Chemical Physics*, vol. 81, no. 1, pp. 511-519, 1984.

[87]   S. Plimpton, "Fast parallel algorithms for short-range molecular dynamics," *J. Comput. Phys.*, vol. 117, no. 1, pp. 1-19, 1995.

[88]   S. Plimpton, A. Thompson, P. Crozier, and A. Kohlmeyer, "LAMMPS molecular dynamics simulator. http://lammps.sandia.gov/.2012.

[89]   A. J. M. Stukowski, "Visualization and analysis of atomistic simulation data with OVITO–the Open Visualization Tool," *Mater. Sci. Eng.*, vol. 18, no. 1, p. 015012, 2009.

[90]   F. Müller-Plathe, "A simple nonequilibrium molecular dynamics method for calculating the thermal conductivity," *J. Chem. Phys.*, vol. 106, no. 14, pp. 6082-6085, 1997.

[91]   I. M. Felix and L. Pereira, "Thermal Conductivity of Graphene-hBN Superlattice Ribbons," *Scientific Reports,* vol. 8, no. 1, p. 2737, 2018.

[92]   P. Erhart and K. Albe, "Analytical potential for atomistic simulations of silicon, carbon, and silicon carbide," *Phys. Rev. B*, vol. 71, no. 3, p. 035211, 2005.

[93]   J. Tersoff, "Modeling solid-state chemistry: Interatomic potentials for multicomponent systems," *Phys. Rev. B*, vol. 39, no. 8, p. 5566, 1989.

[94]   P. Vashishta, R. K. Kalia, A. Nakano, and J. Rino, "Interaction potential for silicon carbide: a molecular dynamics study of elastic constants and vibrational density of states for crystalline and amorphous silicon carbide," *J. Appl. Phys.*, vol. 101, no. 10, p. 103515, 2007

[95]   M. Tang and S. Yip, "Lattice instability in β-SiC and simulation of brittle fracture," *J. Appl. Phys.*, vol. 76, no. 5, pp. 2719-2725, 1994.

[96]   J. Li, L. Porter, and S. Yip, "Atomistic modeling of finite-temperature properties of crystalline β-SiC: II. Thermal conductivity and effects of point defects," *J. Nucl. Mater.*, vol. 255, no. 2-3, pp. 139-152, 1998.

[97]   L. J. Porter, J. Li, and S. Yip, "Atomistic modeling of finite-temperature properties of B-SiC. I. Lattice vibrations, heat capacity, and thermal expansion," *J. Nucl. Mater,* vol. 246, no. 1, pp. 53-59, 1997.

[98]   A. Noreyan, J. Amar, I. Marinescu, "Molecular dynamics simulations of nanoindentation of β-SiC with diamond indenter," *Mater. Sci. Eng.*, vol. 117, no. 3, pp. 235-240, 2005.

[99]   E. Pearson, T. Takai, T. Halicioglu, and W. Tiller, "Computer modeling of Si and SiC surfaces and surface processes relevant to crystal growth from the vapor," *J. Cryst. Growth,* vol. 70, no. 1-2, pp. 33-40, 1984.

[100]   H. Huang, N. M. Ghoniem, J. K. Wong, M. Baskes, "Molecular dynamics determination of defect energetics in beta-SiC using three representative empirical potentials," *Model. Simul. Mater. Sci. Eng.*, vol. 3, no. 5, p. 615, 1995.

[101]   P. C. Andia, F. Costanzo, G. Gray, "A classical mechanics approach to the determination of the stress–strain response of particle systems," *Mater. Sci. Eng.*, vol. 14, no. 4, p. 741, 2006.

[102]   D. Tsai, "The virial theorem and stress calculation in molecular dynamics," *J. Chem. Phys.*, vol. 70, no. 3, pp. 1375-1382, 1979.

[103]   B. Mortazavi and S. Ahzi, "Thermal conductivity and tensile response of defective graphene: A molecular dynamics study," *Carbon*, vol. 63, pp. 460-470, 2013.

[104]   P. Klemens, "Theory of the a-plane thermal conductivity of graphite," *J. Wide Bandgap Mater.*, vol. 7, no. 4, pp. 332-339, 2000.

[105]   E. N. Koukaras, G. Kalosakas, C. Galiotis, and K. Papagelis, "Phonon properties of graphene derived from molecular dynamics simulations," *Scientific Reports*, vol. 5, p. 12923, 2015.

[106]   L. Lindsay, D. Broido, and N. J. P. R. B. Mingo, "Flexural phonons and thermal transport in graphene," vol. 82, no. 11, p. 115427, 2010.

[107]   P. Schelling, "PK Schelling, SR Phillpot, and P. Keblinski, *Phys. Rev. B*, vol. 65, p. 144306, 2002.

[108]   J. Hu, X. Ruan, and Y. Chen, "Thermal conductivity and thermal rectification in graphene nanoribbons: a molecular dynamics study," *Nano Lett.*, vol. 9, no. 7, pp. 2730-2735, 2009.

[109]   J. Che, T. Çağın, W. Deng, and W. Goddard, "Thermal conductivity of diamond and related materials from molecular dynamics simulations," *J. Chem. Phys.*, vol. 113, no. 16, pp. 6888-6900, 2000.

[110]   X. Wu, V. Varshney, J. Lee, Y. Pang, A. K. Roy, and T. Luo, "How to characterize thermal transport capability of 2D materials fairly?–Sheet thermal conductance and the choice of thickness," *Chemical Physics Letters*, vol. 669, pp. 233-237, 2017.

[111]   L. Lindsay, W. Li, J. Carrete, N. Mingo, D. Broido, and T. Reinecke, "Phonon thermal transport in strained and unstrained graphene from first principles," *Phys. Rev. B: Condens. Matter Mater. Phys.*, vol. 89, no. 15, p. 155426, 2014.

[112]   J. M. Ziman, Electrons and phonons: the theory of transport phenomena in solids. *Oxford university press*, 2001.

[113] P. Pichanusakorn, P. Bandaru, "Nanostructured thermoelectrics," *Mater. Sci. Eng. Reports*, vol. 67, no. 2-4, pp. 19-63, 2010.

[114] A. I. Khan, I. A. Navid, M. Noshin, and S. Subrina, "Thermal transport characterization of hexagonal boron nitride nanoribbons using molecular dynamics simulation," *AIP Adv.*, vol. 7, no. 10, p. 105110, 2017.

[115] Zhang X, Xie H, Hu M, Bao H, Yue S, Qin G, Su G. Thermal conductivity of silicene Calculated using an optimized Stillinger-Weber potential. *Phys. Rev B*. 2014; 89: 054310.

[116] Xie H, Hu M, Bao H. Thermal conductivity of silicene from first-principles. *Appl. Phys. Lett.* 2014; 104: 131906.

[117] Landau LD. EM Lifshitz. Statistical Physics. Course of **Theoretical** Physics. 1980; 5: 396-400.